

The orbital evolution of asteroids, pebbles and planets from giant branch stellar radiation and winds

Dimitri Veras^{1*}, Siegfried Eggl², Boris T. Gänsicke¹

¹*Department of Physics, University of Warwick, Coventry CV4 7AL, UK*

²*IMCCE Observatoire de Paris, Univ. Lille 1, UPMC, 77 Av. Denfert-Rochereau, 75014 Paris, France*

Accepted 2015 May 07. Received 2015 May 04; in original form 2015 January 28

ABSTRACT

The discovery of over 50 planets around evolved stars and more than 35 debris discs orbiting white dwarfs highlight the increasing need to understand small body evolution around both early and asymptotic giant branch (GB) stars. Pebbles and asteroids are susceptible to strong accelerations from the intense luminosity and winds of GB stars. Here, we establish equations that can model time-varying GB stellar radiation, wind drag and mass loss. We derive the complete three-dimensional equations of motion in orbital elements due to (1) the Epstein and Stokes regimes of stellar wind drag, (2) Poynting-Robertson drag, and (3) the Yarkovsky drift with seasonal and diurnal components. We prove through averaging that the potential secular eccentricity and inclination excitation due to Yarkovsky drift can exceed that from Poynting-Robertson drag and radiation pressure by at least three orders of magnitude, possibly flinging asteroids which survive YORP spin-up into a widely dispersed cloud around the resulting white dwarf. The GB Yarkovsky effect alone may change an asteroid's orbital eccentricity by ten per cent in just one Myr. Damping perturbations from stellar wind drag can be just as extreme, but are strongly dependent on the highly uncertain local gas density and mean free path length. We conclude that GB radiative and wind effects must be considered when modelling the post-main-sequence evolution of bodies smaller than about 1000 km.

Key words: minor planets, asteroids: general – Kuiper belt: general – stars: AGB and post-AGB – stars: evolution – stars: white dwarfs – planets and satellites: dynamical evolution and stability

1 INTRODUCTION

Robust observational evidence for exoplanetary systems around both main sequence (MS) and post-MS stars demands a self-consistent theory for the formation and late evolution of planetary systems. Although the predominant focus of exoplanetary science has been MS systems, the last decade has seen a surge in interest for giant branch (GB) stars and white dwarfs (WD) that host planetary systems.

1.1 Importance of post-MS planetary systems

The discovery of over 50 exoplanets and nearly 100 substellar companions to stars which have left the main sequence (see Wang et al. 2014, and references therein) help motivate studies which attempt to link the past and future evolution of planetary systems. Detections of these companions have become

more robust with the combined efforts of Doppler radial velocity observations and transit-based photometry (Lillo-Box et al. 2014; Ciceri et al. 2015; Ortiz et al. 2015). Some GB stars contain multiple planets (e.g. Niedzielski et al. 2015), and/or enhanced abundances of lithium, which could represent a key tracer of recent engulfment (Adamów et al. 2012; Nowak et al. 2013; Adamów et al. 2014). Observations of dusty debris discs around subgiant stars (Bonsor et al. 2013, 2014) suggest that collections of material, such as the asteroid belt, can survive the entire MS lifetime of a star.

These observations are bolstered by strong supporting evidence for asteroidal material in WD systems. Although only a few dusty debris discs are known around subgiant stars, over 35 of such discs have been observed orbiting WDs (Zuckerman & Becklin 1987; Becklin et al. 2005; Kilic et al. 2005; Reach et al. 2005; Farihi et al. 2009; Bergfors et al. 2014; Rocchetto et al. 2015). Sometimes accompanying the dust are gaseous components (Gänsicke et al. 2006, 2007, 2008; Gänsicke 2011; Dufour et al. 2012; Farihi et al. 2012; Melis et al. 2012) with both components overlapping radially (Brinkworth et al.

* E-mail: d.veras@warwick.ac.uk

2009; Melis et al. 2010; Brinkworth et al. 2012; Wilson et al. 2014, 2015). The radial extent of these intriguing discs typically does not exceed one Solar radius, which is close to the tidal disruption radius for an asteroid. The environment within this compact region of space is dynamic: the gaseous components of the discs provide kinematic information, and demonstrate sometimes extreme variations with every new observation (Gänsicke et al. 2008; Wilson et al. 2014; Manser et al. 2015). Sharp decreases in luminosity in dusty disc systems also indicate quick drastic changes in the morphology of the circumstellar debris (Xu & Jura 2014).

WDs accrete the disc material, which appear as atmospheric metal abundances, or “pollution”. Any metals heavier than helium sink out of sight on time scales of days to Myrs (depending on the depth of the convection zone), which are in all cases much shorter than the WD cooling age, i.e the time since the star became a WD (see Fig. 1 of Wyatt et al. 2014). Therefore, The detection of photospheric metals implies recent, or ongoing accretion from a circumstellar debris reservoir. Further, between 25 to 50 per cent of all WDs contain signatures of metal pollution (Zuckerman et al. 2003, 2010; Koester et al. 2014), and at widely varying (over 5 Gyr) cooling ages.

1.2 The link between GB and WD planetary systems

These ubiquitously active environments close to WDs must be linked with planetary system evolution during the GB phases of evolution. The interstellar medium is too diffuse to account for amount of metals seen, and is predominately composed of hydrogen. Atmospheric abundances of WDs which are hydrogen-poor and metal-rich (known as DBZ WDs) cannot then arise from the interstellar medium (Aannestad et al. 1993; Friedrich et al. 2004; Jura 2006; Kilic & Redfield 2007; Farihi et al. 2010; Barstow et al. 2014).

The currently-favoured explanation for the origin of atmospheric pollution and debris discs are asteroids which are dynamically perturbed close to the WD and then tidally disrupted there. By asteroids we refer to any objects whose radius is approximately between 0.1km-1000km lying within thousands of au of their parent stars; we denote pebbles and planets as objects with radii between 1mm-1m and larger than 1000km, respectively. Evidence suggests that other potential explanations are unlikely. The accretion and disruption of planets around WDs likely does occur, but too infrequently to explain the large fraction of all WDs currently-observed to be accreting (Veras et al. 2013a; Mustill et al. 2014; Veras & Gänsicke 2015). Exo-Oort cloud comets (with semimajor axes of tens of thousands or hundreds of thousands of au) are unlikely debris progenitors on both chemical (Zuckerman et al. 2007) and dynamical grounds (Veras et al. 2014a), although in isolated cases they may produce detectable accretion (Stone et al. 2015).

Asteroids provide a readily-available reservoir of material with a range of metals diverse enough to help explain the elemental medley observed in atmospheric pollution (Dufour et al. 2012; Gänsicke et al. 2012; Xu et al. 2014). Further, the water retention level in asteroids during the GB phases is uncertain (Jura & Xu 2010, 2012), but might be high enough to explain WDs with water-rich atmospheres (Farihi et al. 2013; Raddi et al. 2015).

Dynamically, asteroids can be scattered onto or close to the

WD through gravitational interactions with surviving planets. Subsequently, the asteroids which avoid direct collisions might tidally disrupt (Graham et al. 1990; Jura 2003; Debes et al. 2012; Bear & Soker 2013; Veras et al. 2014b), creating discs and accreting onto the WD (Rafikov 2011a,b; Rafikov & Garmilla 2012; Wyatt et al. 2014). Some investigations which modelled asteroid perturbations during and beyond GB mass loss have explored different regions of the available phase space, and included one planet in their simulations. These studies encompass Bonsor et al. (2011), who considered asteroids in an exo-Kuiper belt (at 30 au from the star), and Debes et al. (2012) and Frewen & Hansen (2014), who modelled a belt more akin to the asteroid belt (at about a few au from the star).

1.3 Previous most relevant work

None of those three studies included effects from radiation or stellar wind drag in their numerical simulations during GB evolution. However, Veras et al. (2014c) demonstrated that nearly all asteroids with radii between 100m and 10km within about 7 au of their parent star on the MS will later be destroyed because of rotational fission – due to the GB star’s luminosity – from the YORP effect. Consequently, an exo-belt similar to the asteroid belt simply will not survive the GB stellar phases intact, and this phenomenon should be taken into account when modelling asteroid evolution during the WD phases.

Yet, YORP-induced fission is just one consequence of the violent dynamical environment of GB stars. Bonsor & Wyatt (2010) described several others in the context of their influence on debris discs orbiting stars which turn off of the main sequence. The authors considered the effects from Poynting-Robertson drag, and forces they denoted as radiation pressure, stellar wind pressure, and stellar wind drag. Here, we isolate these forces and derive how they change the orbits of small bodies in a general fashion, without making any assumptions about size distributions other than that their diameters are large compared to the wavelength of the incident radiation. We determine, for example, the eccentricity and inclination evolution of orbiting bodies; Bonsor & Wyatt (2010) assumed that the bodies were on circular coplanar orbits.

In addition to Bonsor & Wyatt (2010), Dong et al. (2010) also considered physical effects arising from GB stars. Dong et al. (2010) focused on stellar wind drag and entrainment of small particles along the GB phases, and explicitly included drag in their equations of motion (Stokes regime only), but did not present those equations in orbital elements. They neglected Poynting-Robertson drag, YORP and Yarkovsky¹ effects during AGB evolution, but estimated that those effects would lead to significant orbital evolution - a notion that we quantify in detail here.

Before proceeding with the body of the paper, we present a summary chart (Fig. 1) of the physical effects which should be considered when modeling pebbles, asteroids or planets along different phases of stellar evolution. Boxes without checkmarks indicate forces that are negligible along that particular phase.

This chart simultaneously showcases our conclusions and

¹ Dong et al. (2010) do not make a distinction between the Yarkovsky and YORP effects.

	RADIATION					
	Mass Loss	PR-drag & RP	Yarkovsky	YORP	Wind Drag	
Pebble 1mm -1m		✓				MS
	✓	✓			✓	GB
		✓				WD
Asteroid 1m -1000km		✓	✓	✓		MS
	✓	✓	✓	✓	✓	GB
		✓	✓	✓		WD
Planet > 1000km						MS
	✓					GB
						WD

Figure 1. Effects which are necessary to consider for modeling. The designations MS, GB and WD refer to the main sequence, giant branch and white dwarf phases of stellar evolution. The radiative forces include those from “PR-drag and RP” (Poynting-Robertson drag and radiation pressure; see Section 2.5), the Yarkovsky effect (see Section 2.6), and the YORP effect (see Section 2.2). Properties of stellar winds are introduced in Section 3.3.

reaffirms some results by both Bonsor & Wyatt (2010) and Dong et al. (2010). For example, both studies find that the distribution of pebbles in WD systems will be crucially determined by wind drag along the GB phase. Multiple checkmarks in a single row of Fig. 1 indicate either that multiple forces must be considered together for that stellar phase, or that one may dominate the motion, depending on the physical and orbital variables chosen. Additional forces not included in the chart, such as collisions (Bonsor & Wyatt 2010) or those from additional planets (Dong et al. 2010), can alter the dominant force in a given system during a given phase.

1.4 Outline for this article

Here we determine how GB stars change the orbits of bodies in an all-inclusive fashion under the guise of the perturbed two-body problem. We perform direct comparisons of the effects due to gravity, radiation and drag. We then derive equations of motion in orbital elements through the equation-generation procedure outlined in Veras & Evans (2013a). All of the variables and parameters used are delineated in Tables 1-2 for easy reference. Henceforth, we denote the bodies as *targets* to help avoid any bias towards pebbles, asteroids or planets. Let m represent the target’s fixed mass, \vec{v} the velocity of the target with respect to the star, and \vec{r} the distance between the centre of the target and

the centre of the star². The star has a mass of M which does change with time. The target then evolves according to

$$\frac{d\vec{v}}{dt} = -\frac{G(M(t=0) + m)\vec{r}}{r^3} + \left(\frac{d\vec{v}}{dt}\right)_{\text{ml}} + \left(\frac{d\vec{v}}{dt}\right)_{\text{ra}} + \left(\frac{d\vec{v}}{dt}\right)_{\text{dr}} \quad (1)$$

where the three rightmost terms of equation (1) refer to the contributions from stellar mass loss, radiation, and wind drag. Cartesian formulae for wind drag and mass loss are well-established; radiative effects provide more subtleties. Complete sets of orbital element formulae have been previously described only for mass loss, to our knowledge.

In Section 2, we derive the nontrivial expression for $(d\vec{v}/dt)_{\text{ra}}$ in terms of Cartesian positions and velocities by developing a framework in which to consistently treat Poynting-Robertson drag, radiation pressure, the Yarkovsky effect and YORP. Previous investigations almost exclusively focused on the Solar system. Our treatment here removes the biases of constant luminosity and asteroid belt location which are inherent in those studies.

Section 3 contains our comparison of the magnitudes and relevant size regimes of all of the terms in equation (1). These comparisons of instantaneous accelerations help quantify the relative importance of the different forces at a given time, but not over long times (secular timescales).

In Section 4 we derive the resulting (unaveraged) equations of motion in orbital elements for all of these effects, when viable. We then derive the averaged equations of motion, which reveal secular aspects of the motion. These equations provide a way for us to either compute specific trajectories or place bounds on the motion given our framework in Section 2. We summarize our findings in Section 5.

2 A FRAMEWORK TO MODEL RADIATIVE EFFECTS

Over the last century, the movement of a Solar system object due to radiation pressure has popularly been described through Poynting-Robertson drag (Poynting 1904; Robertson 1937), the Yarkovsky effect (Radzievskii 1954; Peterson 1976) and the YORP (Yarkovsky-O’Keefe-Radzievskii-Paddack) effect (Radzievskii 1954; O’Keefe 1976; Paddack 1969)³. Poynting-Robertson drag and the Yarkovsky effect, which are rarely mentioned in the same context (see Peterson 1976 for an exception),

² This distance is between the centres of the bodies and not their surfaces because we will assume Gauss’ law to calculate the incident radiation on the asteroid. Therefore, as long as the target remains outside of the star’s surface and the stellar emission does not significantly vary over the star’s surface, our equations will hold. Further, the momentum transport equations contain the equivalent cross section of the asteroid, which is assumed to be located where the asteroid has its largest diameter. For a spherical asteroid the cross sectional plane contains the asteroid’s centre.

³ Yarkovsky’s original paper, dating from around 1900, has apparently been lost (Öpik 1951).

Table 1. Roman variables and parameters used in this paper.

Variable	Explanation	Equation #
a	Target's semimajor axis	
A	Target's cross-sectional area (assumed to be $= \pi R^2$ here)	
B	Auxiliary piecewise variable	38
c	Speed of light	
$C_1 - C_{11}$	Auxiliary variables	68, 85
C	Target's specific heat capacity	
d	Target's diameter	
\vec{D}	Auxiliary vectors	86-92
e	Target's eccentricity	
f	Target's true anomaly	
\mathcal{D}	Target's penetration depth scaling	9
G	Gravitational constant	
\vec{h}	Target's specific orbital angular momentum ($= \vec{r} \times \vec{v}$)	
i	Target's inclination with respect to the star's equator	
\mathbb{I}	3x3 unit matrix	
k	Constant between 0 and 1/4	26
K	Target's thermal conductivity	
\mathcal{K}	Constant equal to 0.165	
L	Star's luminosity	
M	Star's mass	
m	Target's mass	
m_{H}	Mass of Hydrogen atom ($\approx 1.66 \times 10^{-27}$ kg)	
n	Target's mean motion	
p	Momentum	
P	Power	
Q_{abs}	Target's absorption efficiency (dimensionless)	
Q_{ref}	Target's reflecting efficiency, or albedo (dimensionless)	
Q_{yar}	Difference of Q_{abs} and Q_{ref} (dimensionless)	
Q_{PR}	Target's radiative efficiency due to Poynting-Robertson drag (dimensionless)	8
\mathbb{Q}	3x3 diagonal radiation matrix	30
\vec{r}	Distance between the centre of the target and the centre of the star	
R	Target's radius	
R_{\star}	Star's radius	
\mathcal{R}	Auxiliary variable	69
\mathbb{R}	General 3x3 rotational orbital matrix	40-48
$\mathbb{R}_1(\vec{s})$	3x3 Rotational matrix #1 for target spin	15
$\mathbb{R}_2(\vec{s})$	3x3 Rotational matrix #2 for target spin	16
$\mathbb{R}_1(\vec{h})$	3x3 Rotational matrix #1 for orbital angular momentum	17
$\mathbb{R}_2(\vec{h})$	3x3 Rotational matrix #2 for orbital angular momentum	18
$\mathbb{R}_Y(\vec{s}, \phi)$	3x3 Rotational matrix for total diurnal Yarkovsky contribution	13
$\mathbb{R}_Y(\vec{h}, \xi)$	3x3 Rotational matrix for total seasonal Yarkovsky contribution	14
Re	Reynolds number of stellar wind at the target's location	39
\vec{s}	Target's spin axis (with angular speed $= \vec{s} $)	3
s_{crit}	Angular speed beyond which bodies in the Solar system with $0.1 \text{ km} \lesssim R \lesssim 10.0$ break up	4
T	Temperature	24
U_{\odot}	A fiducial Solar force ($= 10^{17} \text{ kg m/s}^2$)	3
\vec{v}	Target's velocity with respect to the star	
\vec{v}_{g}	Gas velocity (where the gas is the stellar wind)	
v_{s}	Local sound speed of gas (stellar wind)	
V_{rot}	Star's rotational velocity at its equator	
W	Coefficient of the target's physical asymmetry (dimensionless)	3
\mathbb{Y}	3x3 diagonal Yarkovsky matrix	28
Z	Stellar latitude	25

Table 2. Greek variables and parameters used in this paper.

Variable	Explanation	Equation #
β	Ratio of target's acceleration from radiation to that from gravity	31
γ	Ratio of target's acceleration from radiation to that from mass loss	33
δ	Ratio of target's acceleration from radiation to that from wind drag	57-58
ϵ	Target's emissivity	
ζ	Mean free path length of gas (stellar wind)	
θ	Collision cross-section of gas molecules	
\vec{i}	Relativistically-corrected direction of incoming radiation	6
κ	Auxiliary variable	A1
$\bar{\lambda}$	The peak wavelength of absorbed radiation	
μ	Mean molecular weight	
ξ	Seasonal thermal lag angle in the orbital plane	
Π	Target's orbital period ($= 2\pi/n$)	
ρ	Target's mass density	
ρ_g	Mass density of gas (stellar wind)	
σ	The Stefan-Boltzmann constant	
Σ	Target's rotational spin period ($= 2\pi/ \vec{s} $)	
$\Upsilon_1 - \Upsilon_9$	Auxiliary variables	A6
ϕ	Diurnal thermal lag angle along the target's equator	
Ψ	Mass loss index [$= (dM/dt)/(nM)$]	34
ω	Target's argument of pericentre	
Ω	Target's longitude of ascending node	

both refer to a type of *orbital* recoil effect. YORP instead describes the change in the *spin* of a body due to absorbed radiation. These notions are quantified more precisely in the following subsections.

Although all three effects were originally defined in a Solar system context, their usage and names have been extended to extrasolar systems, and particularly post-main-sequence exosystems (e.g. Rafikov 2011a,b; Veras et al. 2014c). Their applicability to extrasolar systems is at a fundamentally different level partly because of the difference in the precision of available data. Numerous studies (e.g. Kryszczyńska 2013; Rozitis et al. 2013; Jacobson et al. 2014; Lowry et al. 2014; Lupishko & Tielieusova 2014; Polishook 2014; Bottke et al. 2015) performed simulations to match outcomes to known solar system objects at a standard which will be unobtainable in exosystems in the foreseeable future. Therefore, this paper emphasizes placing bounds on the motion and learning as much as possible from the equations of motion, rather than concerning itself with detailed simulation suites. But first, we must create a self-consistent model that is free from the Solar system biases of a constant-luminosity star and asteroids concentrated in location-specific families.

2.1 Goal

Our goal in Section 2 is to find $(d\vec{v}/dt)_{\text{ra}}$, which can be divided into the following three terms

$$\left(\frac{d\vec{v}}{dt}\right)_{\text{ra}} \equiv \left(\frac{d\vec{v}}{dt}\right)_{\text{abs}} + \left(\frac{d\vec{v}}{dt}\right)_{\text{ref}} + \left(\frac{d\vec{v}}{dt}\right)_{\text{yar}}. \quad (2)$$

The first term on the RHS of equation (2) refers to the extra acceleration on the target due to the absorption of radiation. The

second and third terms together give the acceleration due to the re-emission of radiation. The second term refers to re-emission from immediate reflection, and the third term to re-emission from delayed reflection. This delayed reflection is the Yarkovsky effect, and arises from internal thermal redistribution of the absorbed radiation. Note that YORP is absent from equation (2) because it provides no direct orbital acceleration to the target.

2.2 Acceleration due to YORP

Nevertheless, crucially, YORP spins up or down the target. Assume that the target rotates at an angular speed s around its spin axis, defined as $\vec{s} = \{s_x, s_y, s_z\}^T$. Then YORP causes the angular speed to evolve according to (Scheeres 2007)

$$\frac{ds}{dt} = \frac{W}{2\pi\rho R^2} \left(\frac{1}{a^2\sqrt{1-e^2}} \right) \left(U_{\odot} \frac{L(t)}{L_{\odot}} \right) \quad (3)$$

where we gave the star's luminosity L a time dependence for emphasis, $0 \leq W < 1$ is a constant determined by the physical properties (roughly the asymmetry) of the target, R is the target's radius, ρ is the target's density, a is the semimajor axis of the orbit, and e is the eccentricity of the orbit. The term in the last parenthesis comes from Veras et al. (2014c) and represents a fiducial Solar force ($U_{\odot} = 10^{17} \text{ kg m/s}^2$) for application to general extrasolar systems.

Equation (3) is important because it helps determine if a target will undergo fission or survive. In the latter case, the spin evolution could affect the target's acceleration through the Yarkovsky effect, as described in the below sections. Solar system observations show a sharp cutoff for the maximum spin of asteroids with radii approximately between 0.1 km and 10 km

(Harris 1994; Jacobson et al. 2014). This critical spin, s_{crit} , corresponds to a critical breakup period $\Sigma_{\text{crit}} = 2\pi/s_{\text{crit}} \approx 2.33$ hrs. If the target is assumed to be a strengthless rubble pile⁴, then we can express s_{crit} in terms of target density ρ as

$$s_{\text{crit}} \equiv \frac{2\pi}{\sqrt{3\pi/G\rho}} = 7.48 \times 10^{-4} \left(\frac{\rho}{2 \text{ g/cm}^3} \right)^{\frac{1}{2}} \frac{\text{rad}}{\text{s}}. \quad (4)$$

The interplay between the YORP and Yarkovsky effects is complex. For example, YORP may spin up a target quickly enough to activate the Yarkovsky effect. However, if the target is spinning too quickly, it will lose its thermal gradient (or break up). We do not consider the time evolution of the spin in this work.

2.3 Acceleration due to absorbed radiation

The expression for the acceleration due to absorbed radiation is from equation 2 of Burns et al. (2014)

$$\left(\frac{d\vec{v}}{dt} \right)_{\text{abs}} = \frac{AL(t)Q_{\text{abs}}}{4\pi mcr^2} \vec{t} \quad (5)$$

where A is the geometric cross-sectional area of the illuminated surface, Q_{abs} represents the target's absorption efficiency (or, equivalently, fractional amount of energy absorbed that contributes to the momentum transfer), c is the speed of light, and \vec{t} is the relativistically-corrected direction of the incoming radiation to the target such that

$$\vec{t} \equiv \left(1 - \frac{\vec{v} \cdot \vec{r}}{cr} \right) \frac{\vec{r}}{r} - \frac{\vec{v}}{c}. \quad (6)$$

Our equation (5) differs from equation 2 from Burns et al. (2014) because we consider a general extrasolar system with a time-dependent luminosity instead of the Solar constant. Also, Burns et al. (2014) explain that the primed quantities used in their equation are equivalent to the unprimed values in equation (5) to low order in v/c ; this difference in quantities has previously been identified (Klačka et al. 2014).

2.4 Acceleration due to immediately-reflected radiation

The acceleration on the target due to immediately-reflected radiation is expressed in a similar form

$$\left(\frac{d\vec{v}}{dt} \right)_{\text{ref}} = \frac{AL(t)Q_{\text{ref}}}{4\pi mcr^2} \vec{t} \quad (7)$$

where Q_{ref} is the target's reflecting efficiency, or, the fractional amount of energy immediately reemitted after absorption, or simply the albedo. In order to avoid having to account for complex scattering properties of tiny particles, we assume that our targets are at least 100 times the wavelength of radiation (corresponding to the approximate limit between geometric optics and Mie scattering regime).

⁴ Recently, Sánchez & Scheeres (2014) derived spin barriers for bodies which harbour weak cohesive strength due to van der Waals forces between constituent grains. The critical breakup period is similar, but not monotonic as a function of decreasing target radius.

2.5 Acceleration due to Poynting-Robertson drag and “radiation pressure”

Burns et al. (1979) observed that the terms *Poynting-Robertson drag* and *radiation pressure* are ambiguous. Despite how the pressure created by radiation is responsible for *all* of the terms on the RHS of equation (2), plus YORP, the term *radiation pressure* has typically come to mean just the radial component of the sum of $\left(\frac{d\vec{v}}{dt} \right)_{\text{abs}}$ and $\left(\frac{d\vec{v}}{dt} \right)_{\text{ref}}$. Similarly, the term *Poynting-Robertson drag* has typically come to mean just the tangential component of the sum of $\left(\frac{d\vec{v}}{dt} \right)_{\text{abs}}$ and $\left(\frac{d\vec{v}}{dt} \right)_{\text{ref}}$. These components are isolated and discussed in Burns et al. (1979), Mignard (1984) and Hamilton (1993).

Also identified in previous studies is a Q coefficient that is associated with Poynting-Robertson drag, and is already averaged over the stellar spectrum (see e.g. equations 4 and 19 of Burns et al. 1979). This coefficient is related to our formalism through:

$$Q_{\text{PR}} = Q_{\text{abs}} + Q_{\text{ref}}. \quad (8)$$

One must keep in mind that the values of Q are averaged over the stellar spectrum because the stellar spectrum changes with stellar evolutionary phase. Such changes will not cause our conclusions to deviate significantly.

2.6 Acceleration due to the Yarkovsky effect

Now we come to describing the last piece of equation (2), the perturbative acceleration due to the Yarkovsky effect. Recall that the Yarkovsky effect is due to reemission from delayed reflection. The delay comes from the redistribution of thermal energy within the target. Therefore, if the target is too small, or spins very rapidly, no significant temperature differences will occur, and the Yarkovsky effect “turns off”.

2.6.1 Penetration depth

The minimum size of the target at which the effect becomes negligible is approximately the penetration depth scale of the radiation. This depth scale can be derived from a heat conduction model. Here we adopt the simplified 1D model of Brož (2006). This model provides the time lag between insolation and re-emission in realistic materials. The model also assumes that the target rotates at a constant angular speed, and therefore strictly equation (3) cannot be used in conjunction. Realistically, however, YORP spin changes occur relatively slowly compared to thermal wave properties. Therefore, the YORP effect may be included in the model if \vec{s} is considered to be a function of time.

This penetration depth scaling, \mathcal{D} , is

$$\mathcal{D} = \sqrt{\frac{K\Sigma}{\pi\rho\mathcal{C}}} \quad (9)$$

where K is the thermal conductivity and \mathcal{C} is the specific thermal capacity (or specific heat capacity). Hence, the Yarkovsky effect will “turn on” if the target diameter is larger than⁵ \mathcal{D} . As this

⁵ In principle the thermal wave can heat the target by reaching down to its core. In this case, the sufficient condition for the Yarkovsky effect to “turn on” is if the target radius is larger than \mathcal{D} .

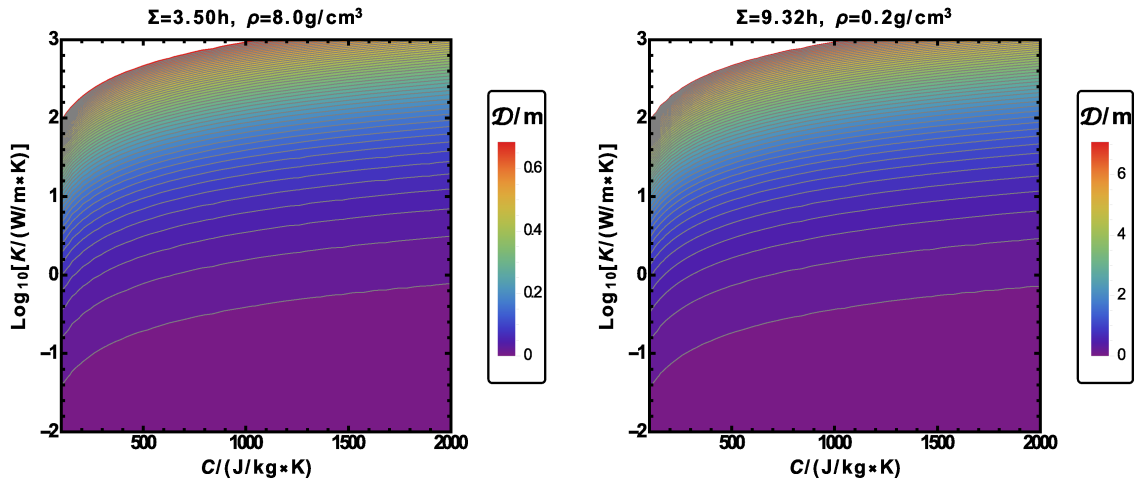


Figure 2. Minimum diameter of target at which the Yarkovsky effect “turns on”. This critical diameter is taken to equal the penetration depth scaling \mathcal{D} , which is a function of the thermal conductivity K and thermal capacity C . The left panel describes a high density ρ target with a fast spin period, equal to $1.5\Sigma_{\text{crit}}$. The right panel instead describes a low density slowly spinning target with $\Sigma = 4.0\Sigma_{\text{crit}}$. The plots bound realistic values of \mathcal{D} to between about 1 cm and 10 m.

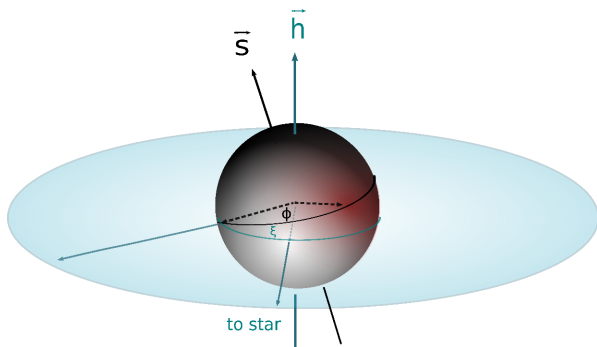


Figure 3. Relevant angles and vectors for the target. The spin axis is \vec{s} , the specific angular momentum axis is \vec{h} , ϕ is the thermal lag angle along the target’s equator, and ξ is the thermal lag angle in the orbital plane. The white spot corresponds to the direction of the star (subsolar point), and the red spot to the maximum of the thermal wave (the direction opposite to the Yarkovsky drift).

scaling significantly depends on the target’s physical properties, we provide contour plots in Fig. 2. The contour plots cover the entire range of possible \mathcal{D} values for both a high density, quickly spinning (left panel) target and a low density, slowly spinning target (right panel). Note that 8 g/cm^3 is slightly higher than the density of iron and 0.2 g/cm^3 is slightly less dense than cork. Target thermal conductivities are confined to $10^{-2} - 10^3 \text{ W/(m}\times\text{K)}$, which include all substances from air to silver. Target specific heat capacities are confined to about $100 \text{ J/(kg}\times\text{K)}$ for heavy metals to about $2000 \text{ J/(kg}\times\text{K)}$ for water. The result, in all cases, is $1 \text{ cm} \lesssim \mathcal{D} \lesssim 10 \text{ m}$, conforming well to Figs. 25-26 of Brož (2006). Therefore, we do not expect Yarkovsky to be active in sub-cm-sized targets, and we expect Yarkovsky to be always active in moderately fast spinning targets larger than 10 m.

2.6.2 Yarkovsky direction

The geometry of the thermal redistribution determines the direction of the Yarkovsky acceleration. This redistribution is dependent on the orientations of both the spin axis \vec{s} and the specific orbital angular momentum axis $\vec{h} = \vec{r} \times \vec{v}$. Let ϕ and ξ represent lag angles of the thermal wave. The variable ϕ represents the thermal lag angle along the target’s equator, i.e. how far the heat wave is dragged along from the subsolar point due to the target’s rotation. The variable ξ represents the thermal lag angle in the orbital plane measured from the subsolar point. See Fig. 3 for a visual representation of these angles.

Solar system studies traditionally denoted the contribution from the spin axis and ϕ as “diurnal” and the contribution from the specific angular momentum axis and ξ as “seasonal”. These characterizations can be traced historically to the thermal imbalance between the morning and afternoon hemispheres (for diurnal) or the winter and summer hemispheres (for seasonal) of a Solar system asteroid. Mathematically, the contributions are expressed via rotation matrices through an angle (here ϕ and ξ) about a given axis (here \vec{s} and \vec{h}) as

$$\left(\frac{d\vec{v}}{dt}\right)_{\text{yar}}^{\text{diurnal}} = \left|\left(\frac{d\vec{v}}{dt}\right)_{\text{yar}}\right| \mathbb{R}_Y(\vec{s}, \phi) \vec{e}, \quad (10)$$

$$\left(\frac{d\vec{v}}{dt}\right)_{\text{yar}}^{\text{seasonal}} = \left|\left(\frac{d\vec{v}}{dt}\right)_{\text{yar}}\right| \mathbb{R}_Y(\vec{h}, \xi) \vec{e}, \quad (11)$$

$$\left(\frac{d\vec{v}}{dt}\right)_{\text{yar}} = \left|\left(\frac{d\vec{v}}{dt}\right)_{\text{yar}}\right| \mathbb{R}_Y(\vec{h}, \xi) \mathbb{R}_Y(\vec{s}, \phi) \vec{e}, \quad (12)$$

where the \mathbb{R} are the following general rotational matrices

$$\mathbb{R}_Y(\vec{s}, \phi) \equiv \cos \phi \mathbb{I} + \sin \phi \mathbb{R}_1(\vec{s}) + (1 - \cos \phi) \mathbb{R}_2(\vec{s}), \quad (13)$$

$$\mathbb{R}_Y(\vec{h}, \xi) \equiv \cos \xi \mathbb{I} - \sin \xi \mathbb{R}_1(\vec{h}) + (1 - \cos \xi) \mathbb{R}_2(\vec{h}) \quad (14)$$

with

$$\mathbb{R}_1(\vec{s}) \equiv \frac{1}{\sqrt{s_x^2 + s_y^2 + s_z^2}} \begin{pmatrix} 0 & -s_z & s_y \\ s_z & 0 & -s_x \\ -s_y & s_x & 0 \end{pmatrix}, \quad (15)$$

$$\mathbb{R}_2(\vec{s}) \equiv \frac{1}{s_x^2 + s_y^2 + s_z^2} \begin{pmatrix} s_x^2 & s_x s_y & s_x s_z \\ s_x s_y & s_y^2 & s_y s_z \\ s_x s_z & s_y s_z & s_z^2 \end{pmatrix}, \quad (16)$$

$$\mathbb{R}_1(\vec{h}) \equiv \frac{1}{\sqrt{h_x^2 + h_y^2 + h_z^2}} \begin{pmatrix} 0 & -h_z & h_y \\ h_z & 0 & -h_x \\ -h_y & h_x & 0 \end{pmatrix}, \quad (17)$$

$$\mathbb{R}_2(\vec{h}) \equiv \frac{1}{h_x^2 + h_y^2 + h_z^2} \begin{pmatrix} h_x^2 & h_x h_y & h_x h_z \\ h_x h_y & h_y^2 & h_y h_z \\ h_x h_z & h_y h_z & h_z^2 \end{pmatrix}. \quad (18)$$

In the specific 1D heat conduction model of Brož (2006), the angles have the following explicit closed forms

$\tan \phi =$

$$\left(1 + \frac{1}{2} \left(\frac{\sigma \epsilon}{\pi^5} \right)^{1/4} \left(\frac{\Sigma}{CK\rho} \right)^{1/2} \left(\frac{L(t)Q_{\text{var}}}{r^2} \right)^{3/4} \right)^{-1}, \quad (19)$$

$\tan \xi =$

$$\left(1 + \frac{1}{2} \left(\frac{\sigma \epsilon}{\pi^5} \right)^{1/4} \left(\frac{\Pi}{CK\rho} \right)^{1/2} \left(\frac{L(t)Q_{\text{var}}}{r^2} \right)^{3/4} \right)^{-1}, \quad (20)$$

where $0 \leq Q_{\text{var}} \leq 1$ is a value satisfying $Q_{\text{abs}} = Q_{\text{ref}} + Q_{\text{var}}$, σ is the Stefan-Boltzmann constant, ϵ is the target's emissivity, and the orbital period Π can be expressed in terms of the target's mean motion n as $\Pi = 2\pi/n = 2\pi a^{3/2}/\sqrt{G(M+m)}$. The angles ϕ and ξ can reach physically meaningful values of between 0° and 45° ; for more details on this result, and the derivation of equations (19-20), see Brož (2006).

2.6.3 Yarkovsky magnitude

Having established the direction of the Yarkovsky acceleration, we now determine the corresponding amplitude. This amplitude may be expressed with momentum p , power P and temperature T using the relativistic energy momentum equation for photons with negligible rest mass as

$$\left| \left(\frac{d\vec{v}}{dt} \right)_{\text{var}} \right| = \frac{1}{m} \frac{dp}{dt} = \frac{\Delta P}{mc} = \frac{1}{mc} [P(T_1) - P(T_2)]. \quad (21)$$

Equation (21) emphasizes that the Yarkovsky effect exists only in the presence of a thermal imbalance on the target's surface. The magnitude of the imbalance is model-dependent. We provide insight into our model by considering the incoming and outgoing power. By assuming radiative balance⁶ we have

⁶ After reaching its equilibrium temperature the target is able to radiate all of the incoming energy eventually, so that it is no longer heating up.

$$P_{\text{in}} = \frac{L(t)A_{\text{in}}Q_{\text{var}}}{4\pi r^2}, \quad (22)$$

$$P_{\text{out}} = A_{\text{out}}\epsilon\sigma T^4. \quad (23)$$

Equating the incoming and outgoing power gives

$$T = \left(\frac{A_{\text{in}}}{A_{\text{out}}} \frac{L(t)Q_{\text{var}}}{4\pi\epsilon\sigma r^2} \right)^{1/4}. \quad (24)$$

The target's equilibrium temperature T depends on ratio of $A_{\text{in}}/A_{\text{out}}$. This ratio is the key to modelling the Yarkovsky effect. Consider first the general case of a fast rotating spherical target with zero obliquity. Because the incoming radiation is directional and the emitted radiation is omnidirectional and symmetric with respect to the equator and the rotation axis, $A_{\text{in}} = \pi R^2$ corresponds to the target's cross section, whereas $A_{\text{out}} = 4\pi R^2$. Alternatively, in the limit of slow rotators (e.g. a 1:1 spin orbit resonance) the target shows always the same hemisphere towards the radiation source (e.g. the Moon as seen from the Earth). In this case, only one hemisphere is constantly heated, and without an atmosphere or unusually high thermal conductivity of the body, only the illuminated hemisphere will be able to emit the incoming energy. Hence, $A_{\text{out}} = 2\pi R^2$ and $A_{\text{in}}/A_{\text{out}} = 1/2$.

In the limit of fast rotation, all of the target's surface elements are heated up to the equilibrium temperature, and hence no strong thermal gradients, and no Yarkovsky effect, is expected. In the limit of slow rotation, because only half of the target's surface can be used as a radiator, the equilibrium temperature on the day side is higher by a factor of $2^{1/4}$ than the equilibrium temperature of the entire target. In this case,

$$\begin{aligned} P(T_1) - P(T_2) &= A_1\epsilon\sigma(2^{1/4}T)^4 - A_2\epsilon\sigma T^4 \\ &= \frac{1}{4} \left(\frac{L(t)A_{\text{in}}Q_{\text{var}}}{4\pi r^2} \right). \end{aligned} \quad (25)$$

where $A_1 = A_2 = A = \pi R^2$ are the momentum-carrying cross-sections of the asteroid's heated and non-heated hemispheres, respectively. However, the violent nature of the GB environment suggests that targets with all types of spins are expected, unless they are far from the star (Veras et al. 2014c). Therefore, generally, the temperature difference will be in between the extremes of 0 and $2^{1/4}T$. Consequently,

$$\left| \left(\frac{d\vec{v}}{dt} \right)_{\text{var}} \right| = \frac{kAL(t)Q_{\text{var}}}{4\pi mcr^2} \quad (26)$$

where $0 \leq k \leq 1/4$. The value of k is strongly linked to the targets's rotation. For objects that spin very fast, i.e. $\Sigma_{\text{crit}} \rightarrow 0$, $k = 0$. Alternatively, for $\Sigma \rightarrow \Pi$, $k = 1/4$.

In the Solar system, the albedo of an asteroid is equal to $(1 - Q_{\text{var}})$. Typical asteroids have albedos between 0.1 and 0.3, meaning that usually Q_{var} is closer to unity than to zero for these objects.

2.6.4 Final result

We now summarize the findings in subsections 2.6.1-2.6.3 and can express the perturbative acceleration due to the Yarkovsky effect as

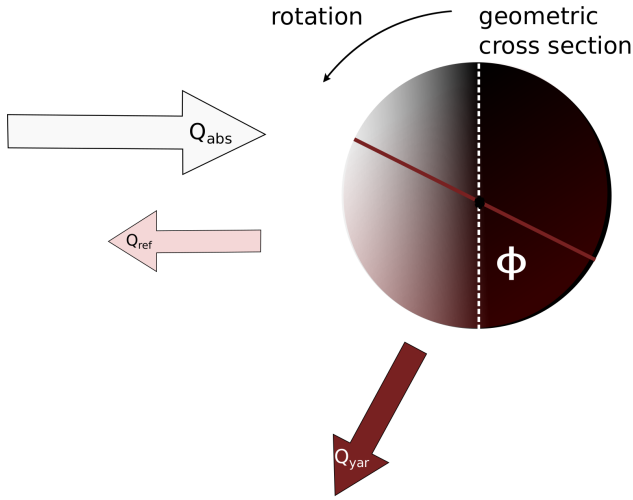


Figure 4. A visual summary of the relevant Q values in equation (29), which represent the efficiency of absorbed radiation (Q_{abs}), immediately reflected radiation (Q_{ref}), and radiation which is reflected after a delay (Q_{yar}). ϕ is the thermal lag angle.

$$\left(\frac{d\vec{v}}{dt}\right)_{\text{yar}} = \frac{kAL(t)Q_{\text{yar}}}{4\pi mcr^2} \mathbb{Y} \vec{r} \quad (27)$$

where

$$\mathbb{Y} \equiv \mathbb{R}_Y(\vec{s}, \phi) \mathbb{R}_Y(\vec{h}, \xi). \quad (28)$$

2.7 Complete expression

Finally we combine equations (5), (7) and (27), along with k from equation (26), into the following single compact expression

$$\left(\frac{d\vec{v}}{dt}\right)_{\text{ra}} = \frac{AL(t)}{4\pi mcr^2} \left[Q_{\text{abs}} \mathbb{I} + Q_{\text{ref}} \mathbb{I} + kQ_{\text{yar}} \mathbb{Y} \right] \vec{r}, \quad (29)$$

where the \mathbb{I} and \mathbb{Y} represent 3x3 matrices (see equation 28). These matrices reveal the relevant regimes of motion. The first term is unchanging and applies for targets of any size. The third term is zeroed out for targets which are too small or do not spin. If those targets are smaller than the typical wavelength of incoming radiation, then only the middle term is affected. The Q quantities in equation (29) are all characterized visually in Figure 4.

3 RELATIVE IMPORTANCE OF DIFFERENT ACCELERATIONS

Now that we have developed an expression that includes all of the effects from radiation, we can estimate the relative importance of radiation compared to mass loss, wind drag and simply unperturbed Keplerian motion at a given time. First, for ease of notation, define the term in brackets from equation (29) as

$$\mathbb{Q} \equiv Q_{\text{abs}} \mathbb{I} + Q_{\text{ref}} \mathbb{I} + kQ_{\text{yar}} \mathbb{Y}. \quad (30)$$

We now describe the physical interpretation of this model. First the asteroid absorbs the momentum of the incoming light with

an efficiency of Q_{abs} . Then part of the radiation is either reflected immediately with an efficiency Q_{ref} and/or thermalized. In the latter case the factor kQ_{yar} determines the relative strength of the Yarkovsky drift.

Because for large bodies ($\lambda \ll d$), $0 \leq Q_{\text{abs}} \leq 1$ and $0 \leq Q_{\text{ref}} \leq 1$, each component of \mathbb{Q} must lie between 0 and 2 inclusive. Generally, $\mathbb{Q} \leq 2$ corresponds to large particles like asteroids only as smaller particles can retain scattering (and thus extinction) cross sections much larger than their geometric cross sections. The Yarkovsky effect has the most importance when $Q_{\text{ref}} = 0$. In this case only a quarter of the total remitted radiative recoil can contribute to the Yarkovsky perturbative acceleration, as $k \leq 1/4$. However, this rudimentary analysis is deceiving, as we will show later with the averaged equations of motion in orbital elements.

3.1 Radiation versus gravity

More broadly, we can develop a sense of when radiative effects are important by comparing the terms on the RHS of equation (1). The first term is the unperturbed two-body term, the second is the acceleration due to mass loss, and the third is the acceleration due to radiation. Define β as the ratio of the radiative acceleration to the total gravitational acceleration, i.e. the ratio of the third term to the sum of the first and second. The sum of the first and second terms is equal to just $-G[M(t) + m]\vec{r}/r^3$, i.e., the first term with a time dependence (Omarov 1962; Hadjidemetriou 1963; Deprit 1983). Then, because $|\vec{r}| \approx 1$ and $|\mathbb{Q}| \leq 2$,

$$\beta \lesssim \frac{AL(t)}{2\pi Gm(M(t) + m)c} \approx \frac{3L(t)}{8\pi GcR\rho M(t)}, \quad (31)$$

an expression which is independent of the semimajor axis a and the eccentricity e .

We plot β in Figure 5 for targets with radii of 1 m (top panel) and 1 mm (bottom panel), corresponding to large and small pebbles. The plots are a function of time, for the entire lifetime of stars with ZAMS (zero-age main sequence) masses of 1.0, 2.0, 3.0, 4.0 and 5.0 M_{\odot} . The variations in each curve are due to the time dependence of both M and L , particularly on the GB phases. We compute stellar evolutionary tracks from the SSE code (Hurley et al. 2000), assuming for all stars Solar metallicity, a Reimers mass loss coefficient of 0.5, and a superwind on the Asymptotic Giant Branch (AGB) phase (Vassiliadis & Wood 1993).

The earlier, minor peak in the curves corresponds to the tip of the Red Giant Branch (RGB) phase, and the later peak the tip of the AGB phase. The figure demonstrates clearly that 1mm-sized targets which remain gravity-dominated for the entire MS and RGB phases will suddenly become radiation-dominated during the AGB phase. This behaviour remains true regardless of the location of the targets. For larger targets which are about one meter in size, the contribution of radiation to their orbital motion along the AGB may reach the one per cent level, potentially enough for example to perturb the targets out of mean motion resonance with another object - a subject for a future study (see e.g. Pástor 2014).

These results must be considered in the appropriate context; they apply only for snapshots of system evolution. In Section 4.3.4 we will show that radiation may in fact dominate the

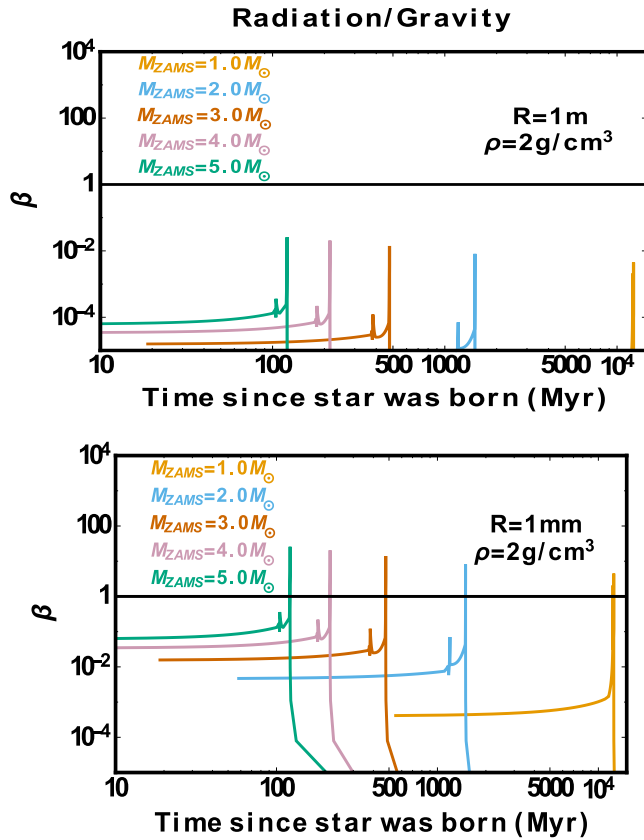


Figure 5. Approximate relative importance of the acceleration due to radiation versus that from gravity (β), as a function of stellar age, for two different pebble-like targets with radii R . The target density of 2 g/cm^3 corresponds to a typical density of an icy Kuiper belt body. Both the stellar mass and luminosity affect β , and vary strongly with time during the GB phases of evolution, causing the peaks in the curves. Particles smaller than about 1 mm will be affected more strongly by radiation than gravity at some point in their evolution.

secular evolution of targets which are orders of magnitude larger than one meter. The reason is due to a potentially accumulating drift from the Yarkovsky effect, which cannot be deduced from the ratio of instantaneous accelerations.

3.2 Radiation versus mass loss

The mass lost by the star, particularly during the GB phases, will contribute to the orbital motion through a change of gravitational potential in the system. We can compare the orbital changes due to radiation to those due specifically to mass loss from equation (1) through

$$\left(\frac{d\vec{v}}{dt}\right)_{\text{ml}} = -\frac{1}{2} \frac{1}{(M(t) + m)} \frac{dM(t)}{dt} \vec{v}. \quad (32)$$

Equation (32) helpfully identifies the acceleration due to isotropic mass loss from the star in terms of positions and velocities (Omarov 1962; Hadjidemetriou 1963; Deprit 1983). Therefore let us define γ as the magnitude of the ratio of the acceleration due to radiation to the acceleration due to mass loss. We obtain

$$\begin{aligned} \gamma &\lesssim \frac{AL(t)M(t)}{\pi m c r^2 v} \left(\frac{dM(t)}{dt}\right)^{-1} \approx \frac{3L}{4\pi R \rho n c r^2 v \Psi(t)} \\ &\approx \frac{3L(t)}{4\pi GM(t)R\rho c \Psi(t)} \left[\frac{(1 + e \cos f)^2}{(1 - e^2)^{3/2} (1 + e^2 + 2e \cos f)^{1/2}} \right], \end{aligned} \quad (33)$$

where

$$\Psi(t) \equiv \frac{1}{nM(t)} \left| \frac{dM(t)}{dt} \right|. \quad (34)$$

In equation (33), we have introduced the true anomaly f and expressed the distance and velocity in terms of orbital elements as

$$r = \frac{a(1 - e^2)}{1 + e \cos f}, \quad (35)$$

$$v = \frac{na}{\sqrt{1 - e^2}} \sqrt{1 + e^2 + 2e \cos f}. \quad (36)$$

The dimensionless mass loss adiabaticity index Ψ is from Veras et al. (2011). This index provides a scaled ratio of the target's orbital period to mass loss timescale, and distinguishes two distinct regimes of motion: adiabatic ($\Psi \ll 1$), when the semimajor axis increases at a constant rate, and runaway ($\Psi \gg 1$), where a , e , and the argument of pericentre ω , increase or decrease at nonuniform rates. This index can be used to determine the evolution of individual known planetary systems (Veras & Wyatt 2012; Mustill et al. 2013; Tadeu dos Santos et al. 2015), isolate the strength of three-body interactions amidst stellar mass loss (Voyatzis et al. 2013), evaluate the contribution of escaped planets to the free-floating planet population (Veras & Raymond 2012), and determine the relative importance of other perturbative effects such as Galactic tides (Veras et al. 2014d). In equation (33) and throughout the paper, we assume that the mass loss is isotropic, an excellent approximation for targets within a few hundred au (Veras et al. 2013b).

Adopting limiting values of f help us understand equation (33). When the target is at pericentre, the term in square brackets becomes $(1 + e)^{-1/2}(1 - e)^{-3/2}$; at apocentre, this term is $(1 - e)^{-1/2}(1 + e)^{-3/2}$. Therefore, for highly eccentric targets, the acceleration from radiation becomes much more important than that from mass loss, more when the target is at pericentre than at apocentre. For moderate or small eccentricities, the bracketed term may be approximated as unity, as for $e = 0.5$, the term approximately equals a value between 0.8 and 2.3. Also, unlike β , γ is dependent on the semimajor axis, through $\Psi(t)$. More generally, the importance of radiation relative to mass loss increases for (i) adiabatic motion, (ii) smaller targets, (iii) less dense targets, and (iv) less massive stars.

We chart γ in Figure 6 for small exobody analogues of the asteroid belt (left panel) and Kuiper belt (right panel). The left and right y -axes in both plots correspond to metre-sized and millimetre-sized targets. We compute the mass loss index in the same manner as in Veras & Tout (2012) and assume Ψ is defined in terms of n rather than Π . This difference has a negligible impact on the resulting curves in the figure, which span several orders of magnitude. We consider the targets at their pericentres; if instead we considered their apocentres, then

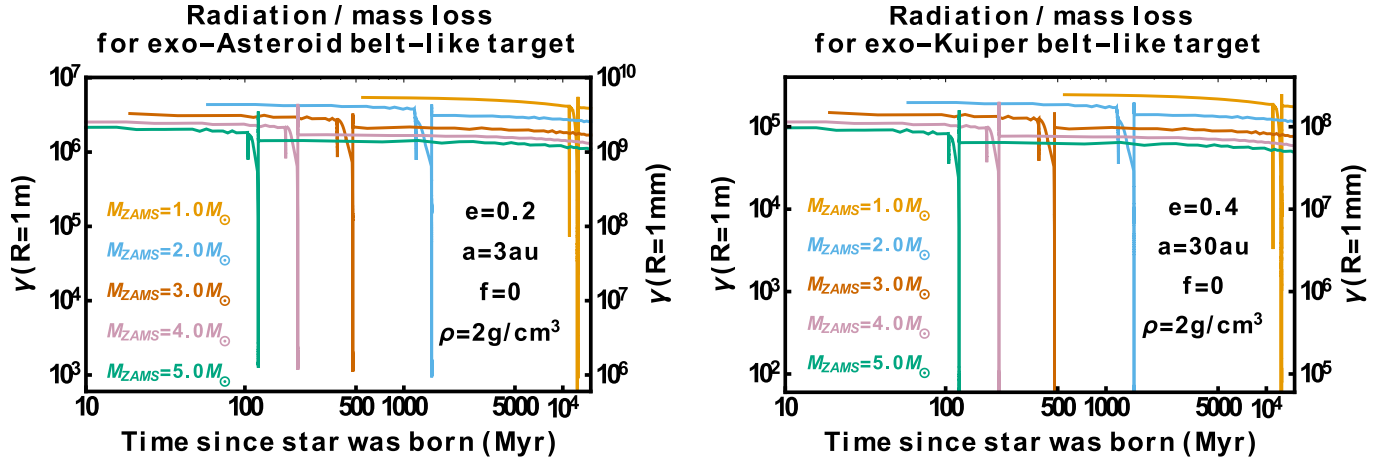


Figure 6. Relative importance of the acceleration due to radiation versus mass loss (γ), as a function of time, for a metre-sized target (left y -axes) and a mm-sized target (right y -axes) in an exo-Asteroid belt (left panel) and in an exo-Kuiper belt (right panel). The variables e , a , f and ρ refer to the target's eccentricity, semimajor axis, true anomaly and mass density, respectively. In all cases, orbital evolution due to radiation is more important than that from stellar mass loss, even at the tip of the AGB phase.

the curves would be shifted downward by factors of $2/3$ (left panel) and $3/7$ (right panel).

The curves suggest that for metre-sized and smaller targets within tens of au, radiation is much more important than mass loss for orbital evolution. Although this ratio is most extreme on the MS, neither radiation nor mass loss contribute much to the unperturbed Keplerian motion (given by the first term on the RHS of equation 1) during this phase. On the AGB phase, this ratio is minimized, but radiation is still more important than mass loss. Therefore, when modelling sub-asteroidal-sized targets along the GB phases, we assert that considering only their orbital evolution due to mass loss is insufficient.

3.3 Radiation versus wind drag

In the previous subsection, we focused on the gravitational evolution due to mass being lost from the two-body orbit. We considered the mass lost to be through a gaseous stellar wind, and ignored the time lag from when the star loses mass to when the ejecta reaches the target. Such subtleties may be unimportant for targets the size of planets, but can be crucial for smaller targets.

3.3.1 The different regimes of wind drag

A solid moving through a gaseous medium will experience a drag force. This well-studied force, in its most basic form, is proportional to the square of the solid's velocity. This form has important applications for protoplanetary discs (e.g. equation 3 of Iwasaki et al. 2002, equations 3-4 of Beaugé et al. 2010, and equation 1 of Yamaguchi & Kimura 2014) but is applicable to a diverse range of systems, including for example the the current Pluto-Charon system environment (equation 3 of Porter & Grundy 2014) and the interstellar medium (equation 3 of Howe & Rafikov 2014). However, the drag coefficient is, in general, not constant. Equations 3.5-3.10 of Adachi et al. (1976) show how the coefficient is actually a function of the Reynolds number, the Mach number and the mean free path length of

the gas molecules. Recent applications which partly rely on results from physical experiments do not all use the same values for the different regimes (see equations 2-4 of Garaud et al. 2004, equations 15-20 of Gibbons et al. 2012, and equations 6-11 of Lorén-Aguilar & Bate 2014), demonstrating slight disagreement.

We use the equations from Garaud et al. (2004), which can be expressed in our notation as

$$\left(\frac{d\vec{v}}{dt}\right)_{\text{dr}} = \begin{cases} \left(\frac{\rho_g v_s}{\rho R}\right) (\vec{v}_g - \vec{v}), & R \ll \zeta \\ \left(\frac{\rho_g B}{\rho R}\right) (\vec{v}_g - \vec{v}) |\vec{v}_g - \vec{v}|, & R \gg \zeta \end{cases} \quad (37)$$

where ρ_g is the density of the gas, ζ is the mean free path length of the gas, $\vec{v}_g = (v_{gx}, v_{gy}, v_{gz})$ is the velocity of the gas, v_s is the local sound speed, and

$$B = \begin{cases} 9 \left[\frac{6R}{\zeta v_s} |\vec{v}_g - \vec{v}| \right]^{-1}, & \text{Re} \leq 1 \\ 9 \left[\frac{6R}{\zeta v_s} |\vec{v}_g - \vec{v}| \right]^{-0.6}, & 1 \leq \text{Re} \leq 800 \\ 0.165, & \text{Re} \geq 800 \end{cases} \quad (38)$$

such that the Reynolds Number Re can be expressed as

$$\text{Re} = \frac{6R}{\zeta v_s} |\vec{v}_g - \vec{v}|. \quad (39)$$

The two pieces of equation (37) refer to the *Epstein regime* (upper relation) and the *Stokes regime* (lower relation).

Equations (37)-(39) should be applicable to GB star winds, just as they would be for protoplanetary discs. In their study of drag in GB systems, Dong et al. (2010) utilize one form of the drag equations in the Stokes regime, and for their model suggest that the drag contribution is much smaller than gravity in the radial, but not necessarily tangential, direction. Bonsor & Wyatt (2010) instead compute a spiral-in timescale due to GB stellar wind drag.

3.3.2 The velocity lag

A key quantity in equations (37)-(39) is the difference in velocity between the gas and target. This difference is also proportional to the Reynolds number (equation 39). Therefore, let us explore this gradient in more detail. Each component of both \vec{v} and \vec{v}_g can be expressed in terms of the target's orbital elements. For \vec{v} , we use equations 5-6 of Veras & Evans (2013a) and define a rotation matrix \mathbb{R} with components

$$\mathbb{R}_{11} = \cos \Omega \cos \omega - \sin \Omega \sin \omega \cos i, \quad (40)$$

$$\mathbb{R}_{21} = \sin \Omega \cos \omega + \cos \Omega \sin \omega \cos i, \quad (41)$$

$$\mathbb{R}_{31} = \sin \omega \sin i, \quad (42)$$

$$\mathbb{R}_{12} = -\cos \Omega \sin \omega - \sin \Omega \cos \omega \cos i, \quad (43)$$

$$\mathbb{R}_{22} = -\sin \Omega \sin \omega + \cos \Omega \cos \omega \cos i, \quad (44)$$

$$\mathbb{R}_{32} = \cos \omega \sin i, \quad (45)$$

$$\mathbb{R}_{13} = \sin \Omega \sin i, \quad (46)$$

$$\mathbb{R}_{23} = -\cos \Omega \sin i, \quad (47)$$

$$\mathbb{R}_{33} = \cos i, \quad (48)$$

where i is the inclination of target's orbit, and Ω and ω are its longitude of ascending node and argument of pericentre. The target's velocity components are then

$$\vec{v} \equiv \mathbb{R} \begin{pmatrix} \frac{-na \sin f}{\sqrt{1-e^2}} \\ \frac{na(e+\cos f)}{\sqrt{1-e^2}} \\ 0 \end{pmatrix}. \quad (49)$$

The velocity of the gas (or wind) is assumed to be constant and in the radial direction. This velocity is dictated entirely by the star, but shares the same space, and geometry, of the target. Consequently, we may express the components of \vec{v}_g at the target's location in terms of the orbital parameters of the target as (equation 2.122 of Murray & Dermott 1999)

$$v_{gx} = |\vec{v}_g| [\cos \Omega \cos (\omega + f) - \sin \Omega \sin (\omega + f) \cos i], \quad (50)$$

$$v_{gy} = |\vec{v}_g| [\sin \Omega \cos (\omega + f) + \cos \Omega \sin (\omega + f) \cos i], \quad (51)$$

$$v_{gz} = |\vec{v}_g| [\sin (\omega + f) \sin i]. \quad (52)$$

Equations (49)-(51) state that the gas velocity is in the radial direction. However, we must carefully consider the context when applying equations (50)-(52). For example, they would be incongruous if inserted into averaged equations of motion.

The magnitude of \vec{v}_g is dictated by the physical properties of the star. Because the launching mechanism of the wind is unknown (Bladh & Höfner 2012) and may vary as a function of stellar evolution (see Owocki 2004 for a review), we can make only an approximation. We approximate the ejecta speed as a function of the star's latitude as (Owocki 2013)

$$|\vec{v}_g| = \sqrt{\left(\frac{2GM}{R_\star(t)}\right) \left(1 - \frac{R_\star(t)V_{\text{rot}}(t)^2}{GM} \cos^2 Z\right)}, \quad (53)$$

where R_\star is the radius of the star, Z is latitude, and V_{rot} is the rotational velocity of the star at the equator. Time dependencies

are included to emphasize the potentially significant variance of these quantities along the GB phases. MS stars do also have winds, but for fixed values of R_\star and V_{rot} . WD stars have not yet been observed to emit winds, and therefore in this context the concept of gas drag through stellar winds does not exist and equation (53) is not applicable.

3.3.3 The gas density, mean free path length, and sound speed

Before proceeding, we must make some approximations about the gas density ρ_g , the mean free path length (which we denote as ζ), and the sound speed v_s . If the wind is spherically symmetric so that ρ_g can be determined from the mass loss rate, then we can write (equation 5 of Dong et al. 2010)

$$\frac{dM(t)}{dt} = 4\pi r^2 \rho_g |\vec{v}_g|. \quad (54)$$

With a given mass loss rate, and a gas velocity given by equation (53), one can determine ρ_g .

Given an expression for ρ_g , how can we determine ζ ? These quantities are related through

$$\zeta = \frac{\mu m_H}{\theta \rho_g}, \quad (55)$$

where μ is the mean molecular mass of the gas (or stellar wind), m_H is the mass of a Hydrogen atom, and θ is the collision cross-section of the gas molecules. In equation (55), m_H is fixed and μ is on the order of unity, so we need to bound the collisional cross-section θ . Based on the known radii of chemical elements, $10^{-20} \text{m}^2 \lesssim \theta \lesssim 10^{-18} \text{m}^2$. Consequently, we make the approximate relation

$$\rho_g \zeta \sim 10^{-8} \text{kg/m}^2. \quad (56)$$

By using this relation, we plot ζ in Figure 7. The plot illustrates how at a fixed point in space, ζ will vary by many orders of magnitude during the GB phase. ζ is minimized at the tip of the AGB, and scales with the square of the distance to the star.

The sound speed v_s is also unknown, and is a function of the properties of the changing wind. Owocki (2014) suggests that v_s is a small fraction (~ 0.001) of the escape velocity of the wind from the star. For simplicity and for lack of better constraints, we will assume that v_s is constant and given by this ratio.

3.3.4 The Reynolds number

Having now established methods or values for obtaining ζ and v_s , we can attempt to estimate the Reynolds number (equation 39). The Reynolds number is particularly important because it defines the flow regime in which the target resides. Figure 8 demonstrates how the variation in Re can be great enough for a fixed point in space to be subject to several different flow regimes throughout GB evolution.

3.3.5 Comparing wind drag with radiation

Having obtained some physical intuition for the variation of the Reynolds number, we can now finally consider the acceleration due to wind drag. In the same vein as we have defined β and γ , here let us define δ as the ratio of the perturbative acceleration

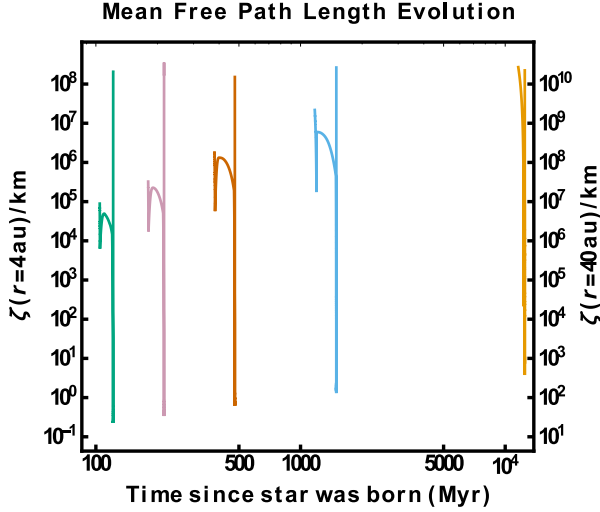


Figure 7. Evolution of the mean free path length of the stellar wind for a fixed-in-space target across the giant branch phases of stellar evolution. The target’s physical and orbital parameters are $R = 1$ cm, $a = 5$ au (left y -axis), $a = 50$ au (right y -axis), $e = 0.2$, $i = 0^\circ$, $\Omega = \omega = f = 0^\circ$. The plot demonstrates how ζ undergoes changes of over 5 orders of magnitude, and achieves a minimum at the tip of the AGB.

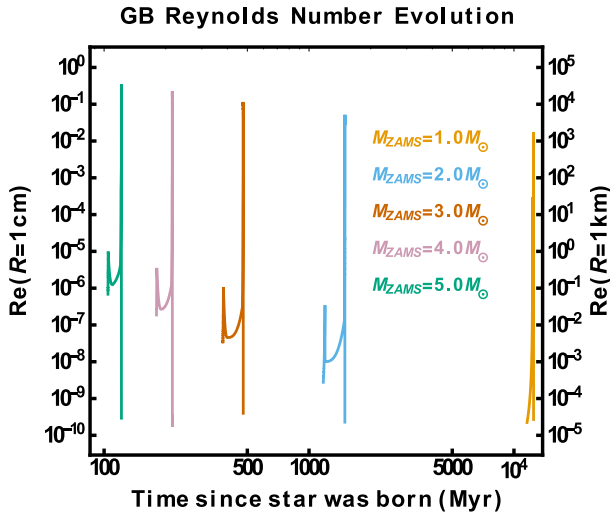


Figure 8. Evolution of the Reynolds number of the stellar wind for a fixed-in-space target across the giant branch phases of stellar evolution. The target’s orbital parameters are $a = 5$ au, $e = 0.2$, $i = 0^\circ$, $\Omega = \omega = f = 0^\circ$. The left and right y -axes respectively illustrate the evolution for a $R = 1$ cm pebble-like target and a $R = 1$ km asteroid-like target. The asteroid traverses all three of the Stokes flow regimes (equation 38).

due to radiation to the perturbative acceleration due to wind drag. In the Epstein regime,

$$\delta \approx \frac{3L(1+e\cos f)^2}{8\pi c a^2 (1-e^2)^2 \rho_g |\vec{v}_g|} |\vec{v}_g - \vec{v}|^{-1}$$

Radiation/wind drag

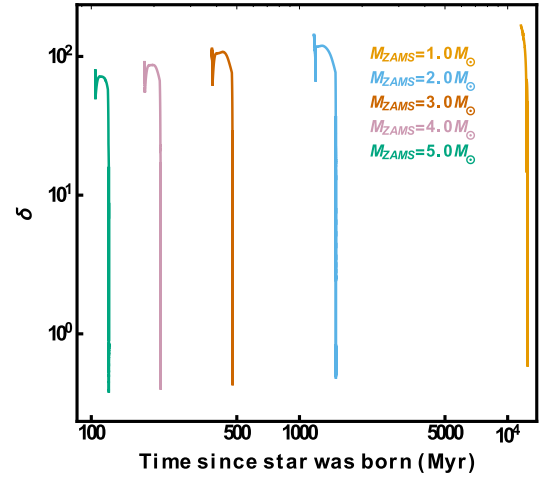


Figure 9. Relative importance of radiation versus wind drag for a fixed-in-space target across the giant branch phases of stellar evolution. The $R = 1$ cm target has orbital parameters of $a = 5$ au, $e = 0.2$, $i = 0^\circ$, and $\Omega = \omega = f = 0^\circ$. However, the evolution of δ is largely insensitive to any of these parameters and is instead largely determined by the competition between the mass and luminosity evolution of the star (equations 57 and 58).

$$= \frac{3L}{2c |\vec{v}_g - \vec{v}|} \left(\frac{dM}{dt} \right)^{-1} \quad (57)$$

whereas in the Stokes regime

$$\begin{aligned} \delta &\approx \frac{3L(1+e\cos f)^2}{8\pi c a^2 (1-e^2)^2 \rho_g B} |\vec{v}_g - \vec{v}|^{-2} \\ &= \frac{3L |\vec{v}_g|}{2c B |\vec{v}_g - \vec{v}|^2} \left(\frac{dM}{dt} \right)^{-1}. \end{aligned} \quad (58)$$

The simplification we performed in equations (57)-(58) holds only when one assumes the spherically symmetric wind of equation (54). In this approximation, δ is largely independent of the target’s location or size, and instead is dependent almost entirely on the properties of the star. Figure 9 illustrates the evolution of δ for the stellar models that we adopted. The curves suggest that the competition between radiation and wind drag is close, and both should be considered together in GB planetary studies.

3.4 Comparison of all forces together

Having defined the dimensionless ratios β , γ and δ , we can now compare the strength of mass loss, gravity, wind drag and radiation at given snapshots of time. See Figure 10. In all cases, radiation and wind drag are comparable in strength, and comparable at all target radii sampled. Recall that δ is independent of R everywhere except when the target is in the Stokes regime and $\text{Re} \leq 800$. However, the pebble (with $\text{Re} \sim 10^{-9} - 10^{-2}$) and asteroid (with $\text{Re} \sim 10^{-4} - 10^3$) are both always in the Epstein regime here, and when the planet (with $\text{Re} \sim 10^0 - 10^7$) is in the Stokes regime, usually $\text{Re} > 800$. Consequently, changes in the purple dotted lines are almost indiscernible. Expectedly, gravity

dominates the evolution of planet-sized targets, and mass loss becomes relatively more important the further one moves away from the star. These trends vary little for different progenitor stellar masses.

Although broadly useful, this type of comparison does not (i) characterize the evolution of individual orbital elements (such as eccentricity), and (ii) fails to account for cumulative effects. Consequently, the middle panels suggest that gravity will dominate the evolution of asteroids. These plots do not reveal that the long-term effect of the (radiative) Yarkovsky force can excite an asteroid's orbit to instability, as shown in Section 4.3.4. These plots are primarily useful for order of magnitude estimates and short-term evolution; detailed evolutionary models should instead rely on Figure 1.

4 EQUATIONS OF MOTION IN ORBITAL ELEMENTS

The physical intuition gained in the last section from the comparison of forces provides a foundation for the more precise treatment that we supply here. We seek to express the equations of motions due to wind drag and radiation entirely in terms of orbital elements through the formalism first mentioned in Veras et al. (2011) and developed in Veras & Evans (2013a). Based on work by Efroimsky (2005b) and Gurfil (2007), Veras & Evans (2013a) delineated how one can derive orbital-element-only equations from a two-body problem with a perturbation expressed entirely in terms of Cartesian elements, without any averaging. This procedure assumes only boundedness of the orbits, and otherwise does not make any assumptions about the magnitude of the perturbation or the resulting orbital elements.

Among the benefits of this task is the ability to then average over the result to create a new set of equations which can be integrated much more quickly and provide perspective on the target's secular evolution. Further, for the particular case of perturbations due to radiation, we will demonstrate that in some cases averaged leading-order terms vanish, helping to provide a better assessment of the orbital changes than those from Figs. 5 and 6. Henceforth, for ease of notation, we drop the explicit dependence of time on M and L .

Unlike the other variables, the time evolution of the true anomaly need not be split up by type of force. The following relation holds true individually for mass loss, wind drag and radiative forces, and together for the overall evolution

$$\frac{df}{dt} = \frac{n(1 + e \cos f)^2}{(1 - e^2)^{3/2}} - \frac{d\omega}{dt} - \cos i \frac{d\Omega}{dt}. \quad (59)$$

The true anomaly also represents the variable over which we average in order to obtain the secular equations.

4.1 Mass loss equations

First, for completeness and comparison, we repeat the known isotropic mass loss equations. Mass loss significantly changes the orbits of targets of all sizes.

4.1.1 Unaveraged equations

The unaveraged equations of motion in orbital elements for isotropic mass loss are (Omarov 1962; Hadjidemetriou 1963; Veras et al. 2011)

$$\left(\frac{da}{dt}\right)_{\text{ml}} = -\frac{a(1 + e^2 + 2e \cos f)}{1 - e^2} \frac{1}{M + m} \frac{dM}{dt}, \quad (60)$$

$$\left(\frac{de}{dt}\right)_{\text{ml}} = -(e + \cos f) \frac{1}{M + m} \frac{dM}{dt}, \quad (61)$$

$$\left(\frac{di}{dt}\right)_{\text{ml}} = 0, \quad (62)$$

$$\left(\frac{d\Omega}{dt}\right)_{\text{ml}} = 0, \quad (63)$$

$$\left(\frac{d\omega}{dt}\right)_{\text{ml}} = -\frac{\sin f}{e} \frac{1}{M + m} \frac{dM}{dt}. \quad (64)$$

The more complex anisotropic equations of motion (Veras et al. 2013b) in fact more realistically represent the motion, but, as previously suggested, they provide a negligible improvement on equations (60-64) except in extreme cases.

4.1.2 Averaged equations

We obtain averages by performing the following integral for each variable (here for averaged semimajor axis change due to mass loss)

$$\left\langle \left(\frac{da}{dt}\right)_{\text{ml}} \right\rangle = \frac{1}{2\pi} \int_0^{2\pi} \left(\frac{da}{dt}\right)_{\text{ml}} \frac{(1 - e^2)^{3/2}}{(1 + e \cos f)^2} df. \quad (65)$$

We find that all secular motions vanish except for the semimajor axis:

$$\left\langle \left(\frac{da}{dt}\right)_{\text{ml}} \right\rangle = -\frac{a}{M + m} \frac{dM}{dt}, \quad (66)$$

$$\left\langle \left(\frac{de}{dt}\right)_{\text{ml}} \right\rangle = \left\langle \left(\frac{d\omega}{dt}\right)_{\text{ml}} \right\rangle = 0. \quad (67)$$

The averaging assumes that dM/dt is a constant and is much less than df/dt , such that $M(t)$ is also approximately constant on orbital timescales. Equations (66)-(67) represent an excellent approximation for targets within hundreds of au (Veras et al. 2011).

4.2 Wind drag equations

Our derivation of the wind drag equations of motion in orbital elements make no assumption about $\vec{v}_g = (v_{gx}, v_{gy}, v_{gz})$. The gas velocity here does not have to adhere to the prescriptions in equations (50)-(53) nor equation (54).

4.2.1 Auxiliary expressions

In order to express our equations in a compact manner, we define a standard set of auxiliary variables that appear regularly in studies of the perturbed two-body problem (Veras et al. 2013b; Veras & Evans 2013a,b; Veras 2014a).

Comparison of all effects
(dot-dashed $\equiv 1/\beta$, dashed $\equiv 1/\gamma$, dotted $\equiv 1/\delta$)

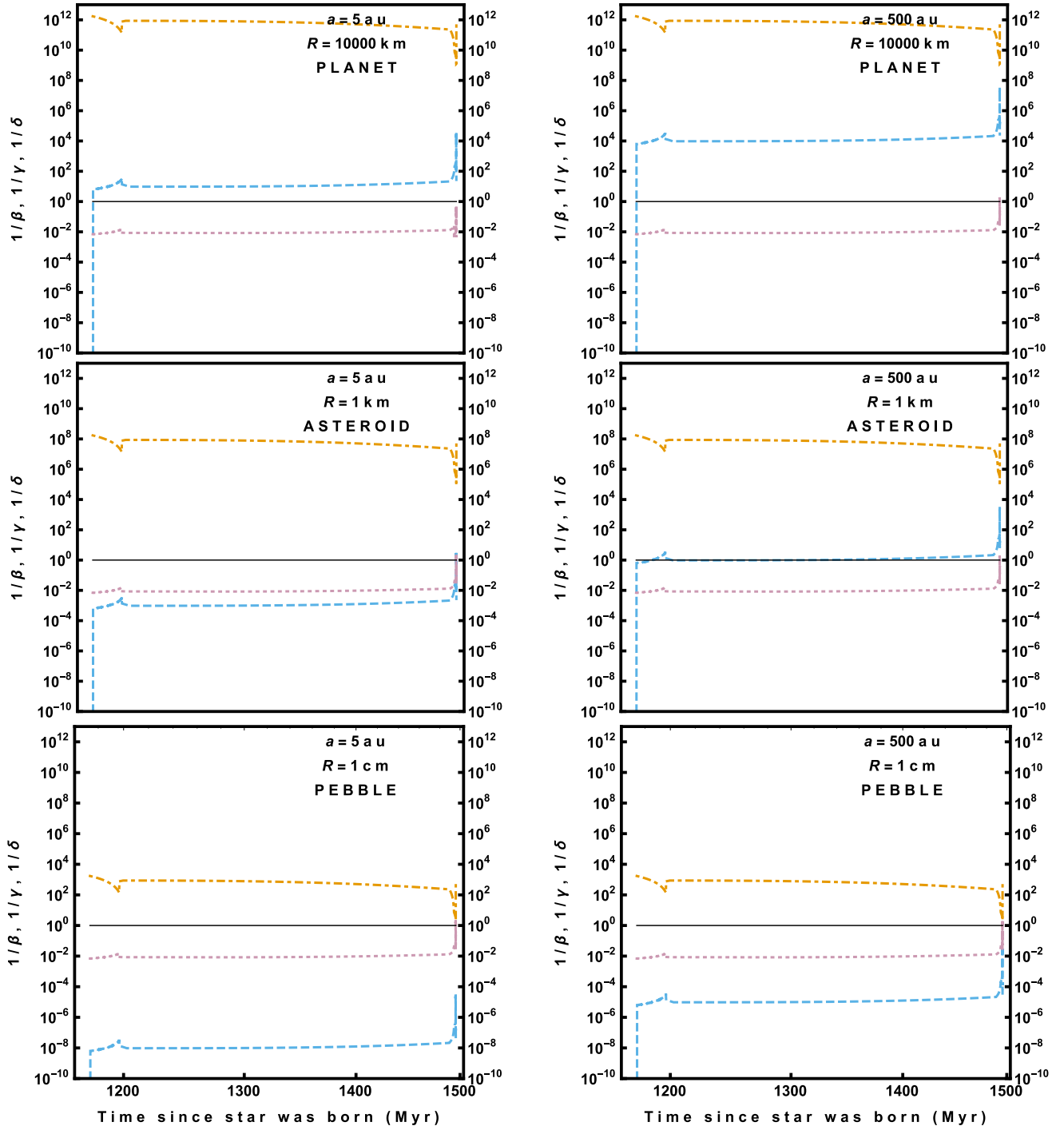


Figure 10. Relative instantaneous acceleration strengths of gravity ($1/\beta$; orange dot-dashed lines), mass loss ($1/\gamma$; blue dashed lines), and wind drag ($1/\delta$; purple dotted lines), all compared to radiation for $M_{\text{ZAMS}} = 2M_{\odot}$ stars along the GB phases. The relative strengths and profile features for other progenitor stellar masses are similar. The top, middle and bottom panels illustrate targets which are a planet, asteroid and pebble, and the left and right panels represent locations given by $a = 5 \text{ au}$ and $a = 500 \text{ au}$ assuming the target is on a circular coplanar orbit. This plot represents just a snapshot in time and does not take into account potentially large long-term accumulations; detailed models should instead consider all checked forces from Table 1.

$$\begin{aligned}
C_1 &\equiv e \cos \omega + \cos(f + \omega) \\
C_2 &\equiv e \sin \omega + \sin(f + \omega) \\
C_3 &\equiv \cos i \sin \Omega \sin(f + \omega) - \cos \Omega \cos(f + \omega) \\
C_4 &\equiv \cos i \cos \Omega \sin(f + \omega) + \sin \Omega \cos(f + \omega) \\
C_5 &\equiv (3 + 4e \cos f + \cos 2f) \sin \omega \\
&\quad + 2(e + \cos f) \cos \omega \sin f \\
C_6 &\equiv (3 + 4e \cos f + \cos 2f) \cos \omega \\
&\quad - 2(e + \cos f) \sin \omega \sin f \\
C_7 &\equiv (3 + 2e \cos f - \cos 2f) \cos \omega + \sin \omega \sin 2f \\
C_8 &\equiv (3 - \cos 2f) \sin \omega - 2(e + \cos f) \cos \omega \sin f \\
C_9 &\equiv (3 + 2e \cos f - \cos 2f) \sin \omega - \cos \omega \sin 2f.
\end{aligned} \tag{68}$$

Additionally, in the following derivations we found that a commonly-occurring quantity is

$$\begin{aligned}
\mathcal{R} &\equiv \left\{ \left(v_{\text{gx}} + \frac{an(C_2 \cos \Omega + C_1 \sin \Omega \cos i)}{\sqrt{1-e^2}} \right)^2 \right. \\
&\quad + \left(v_{\text{gy}} + \frac{an(-C_1 \cos i \cos \Omega + C_2 \sin \Omega)}{\sqrt{1-e^2}} \right)^2 \\
&\quad \left. + \left(v_{\text{gz}} - \frac{anC_1 \sin i}{\sqrt{1-e^2}} \right)^2 \right\}^{1/5}.
\end{aligned} \tag{69}$$

4.2.2 Unaveraged equations for Epstein regime

Recall that in the following derivations, we make no assumptions about \vec{v}_g . Consequently, from equation (37) we obtain

$$\begin{aligned}
\left(\frac{da}{dt} \right)_{\text{dr}} &= \frac{2v_s \rho_g}{nR\rho(1-e^2)} \left\{ -an(1+e^2+2e \cos f) \right. \\
&\quad + \sqrt{1-e^2} \left[v_{\text{gz}} C_1 \sin i + v_{\text{gy}} (C_1 \cos i \cos \Omega - C_2 \sin \Omega) \right. \\
&\quad \left. \left. - v_{\text{gx}} (C_1 \cos i \sin \Omega + C_2 \cos \Omega) \right] \right\},
\end{aligned} \tag{70}$$

$$\begin{aligned}
\left(\frac{de}{dt} \right)_{\text{dr}} &= -\frac{v_s \rho_g}{2anR\rho(1+e \cos f)} \left\{ 4aen \right. \\
&\quad + 4an \cos f (1+e^2+e \cos f) + \sqrt{1-e^2} \left[-v_{\text{gz}} C_6 \sin i \right. \\
&\quad + v_{\text{gy}} (-C_6 \cos i \cos \Omega + C_5 \sin \Omega) \\
&\quad \left. \left. + v_{\text{gx}} (C_6 \cos i \sin \Omega + C_5 \cos \Omega) \right] \right\},
\end{aligned} \tag{71}$$

$$\begin{aligned}
\left(\frac{di}{dt} \right)_{\text{dr}} &= \frac{\sqrt{1-e^2} v_s \rho_g \cos(f + \omega)}{anR\rho(1+e \cos f)} \\
&\quad \times [v_{\text{gz}} \cos i - v_{\text{gy}} \sin i \cos \Omega + v_{\text{gx}} \sin i \sin \Omega],
\end{aligned} \tag{72}$$

$$\begin{aligned}
\left(\frac{d\Omega}{dt} \right)_{\text{dr}} &= \frac{\sqrt{1-e^2} v_s \rho_g \sin(f + \omega)}{anR\rho(1+e \cos f)} \\
&\quad \times [v_{\text{gz}} \cot i - v_{\text{gy}} \cos \Omega + v_{\text{gx}} \sin \Omega],
\end{aligned} \tag{73}$$

$$\begin{aligned}
\left(\frac{d\omega}{dt} \right)_{\text{dr}} &= -\frac{v_s \rho_g}{4anR\rho e \sqrt{1-e^2} (1+e \cos f)} \left\{ \right. \\
&\quad 8an \sqrt{1-e^2} (1+e \cos f) \sin f - 2(1-e^2) \\
&\quad \times \left[-v_{\text{gz}} [C_9 \sin i + 2e \cos i \cot i \sin(f + \omega)] \right. \\
&\quad - v_{\text{gy}} (C_8 \cos i \cos \Omega + C_7 \sin \Omega) \\
&\quad \left. \left. + v_{\text{gx}} (-C_7 \cos \Omega + C_8 \cos i \sin \Omega) \right] \right\}.
\end{aligned} \tag{74}$$

Equations (70)-(74) reveal that all the orbital elements vary along a single orbit due to Epstein drag, even if the orbit is initially eccentric or circular. This fact remains true even if spherical symmetry is imposed.

4.2.3 Unaveraged equations for Stokes regime, $Re \leq 1$

The orbital element evolution equations of motion in this regime are equivalent to those in Section 4.2.2, but with right-hand-sides multiplied by a factor of $3\zeta/2R$. Recall that targets will rarely find themselves in this regime, and must be close to the star to do so.

4.2.4 Unaveraged equations for Stokes regime, $1 \leq Re \leq 800$

The equations of motion in this subregime have a similar form to those in Section 4.2.2, but are scaled differently.

$$\begin{aligned}
\left(\frac{da}{dt} \right)_{\text{dr}} &= -\frac{3 \cdot 6^{2/5} \zeta^{3/5} v_s^{3/5} \rho_g \mathcal{R}}{\sqrt{an\rho(1-e^2)} R^{8/5}} \\
&\quad \times \left\{ na^{3/2} (1+e^2+2e \cos f) + a\sqrt{1-e^2} \right. \\
&\quad \left[-v_{\text{gz}} C_1 \sin i + v_{\text{gy}} (-C_1 \cos i \cos \Omega + C_2 \sin \Omega) \right. \\
&\quad \left. \left. + v_{\text{gx}} (C_1 \cos i \sin \Omega + C_2 \cos \Omega) \right] \right\},
\end{aligned} \tag{75}$$

$$\begin{aligned}
\left(\frac{de}{dt} \right)_{\text{dr}} &= -\frac{3^{7/5} \zeta^{3/5} v_s^{3/5} \rho_g \mathcal{R}}{2^{8/5} a^{3/2} n \rho (1+e \cos f) R^{8/5}} \\
&\quad \times \left\{ 2a^{3/2} n [2 \cos f (1+e^2) + e(3 + \cos 2f)] + a\sqrt{1-e^2} \right. \\
&\quad \left[-v_{\text{gz}} C_6 \sin i + v_{\text{gy}} (-C_6 \cos i \cos \Omega + C_5 \sin \Omega) \right. \\
&\quad \left. \left. + v_{\text{gx}} (C_6 \cos i \sin \Omega + C_5 \cos \Omega) \right] \right\},
\end{aligned} \tag{76}$$

$$\left(\frac{di}{dt}\right)_{\text{dr}} = \frac{3^{7/5} \zeta^{3/5} v_s^{3/5} \rho_g \mathcal{R} \sqrt{1-e^2} \cos(f+\omega)}{2^{3/5} a n \rho (1+e \cos f) R^{8/5}} \times \left\{ v_{gz} \cos i - v_{gy} \sin i \cos \Omega + v_{gx} \sin i \sin \Omega \right\}, \quad (77)$$

$$\left(\frac{d\Omega}{dt}\right)_{\text{dr}} = \frac{3^{7/5} \zeta^{3/5} v_s^{3/5} \rho_g \mathcal{R} \sqrt{1-e^2} \sin(f+\omega)}{2^{3/5} a n \rho (1+e \cos f) R^{8/5}} \times \left\{ v_{gz} \cot i - v_{gy} \cos \Omega + v_{gx} \sin \Omega \right\}, \quad (78)$$

$$\left(\frac{d\omega}{dt}\right)_{\text{dr}} = -\frac{3^{7/5} \zeta^{3/5} v_s^{3/5} \rho_g \mathcal{R}}{2^{8/5} a n e \sqrt{1-e^2} \rho (1+e \cos f) R^{8/5}} \times \left\{ 4a n \sqrt{1-e^2} \sin f (1+e \cos f) - (1-e^2) \right. \\ \times \left[-v_{gz} (C_9 \sin i + 2e \cos i \cot i \sin(f+\omega)) \right. \\ \left. - v_{gy} (C_8 \cos i \cos \Omega + C_7 \sin \Omega) \right. \\ \left. \left. + v_{gx} (C_8 \cos i \sin \Omega - C_7 \cos \Omega) \right] \right\}. \quad (79)$$

4.2.5 Unaveraged equations for Stokes regime, $800 \leq Re$

In this subregime, B is a constant. Let $B = 0.165 \equiv \mathcal{K}$. Although the equations simplify and $(di/dt)_{\text{dr}}$ and $(d\Omega/dt)_{\text{dr}}$ vanish, the remaining equations are still not generally solvable analytically.

The full equations are

$$\left(\frac{da}{dt}\right)_{\text{dr}} = -\frac{2\mathcal{K}\rho_g \mathcal{R}^{5/2}}{nR\rho(1-e^2)} \left\{ a n (1+e^2 + 2e \cos f) \right. \\ \left. + \sqrt{1-e^2} \left[-v_{gz} C_1 \sin i + v_{gy} (-C_1 \cos \Omega \cos i + C_2 \sin \Omega) \right. \right. \\ \left. \left. + v_{gx} (C_1 \sin \Omega \cos i + C_2 \cos \Omega) \right] \right\}, \quad (80)$$

$$\left(\frac{de}{dt}\right)_{\text{dr}} = -\frac{\mathcal{K}\rho_g \mathcal{R}^{5/2}}{2naR\rho(1+e \cos f)} \times \left\{ 2a n [3e + 2(1+e^2) \cos f + e \cos(2f)] \right. \\ \left. + \sqrt{1-e^2} \left[-v_{gz} C_6 \sin i \right. \right. \\ \left. + v_{gy} (-C_6 \cos \Omega \cos i + C_5 \sin \Omega) \right. \\ \left. \left. + v_{gx} (C_6 \sin \Omega \cos i + C_5 \cos \Omega) \right] \right\}, \quad (81)$$

$$\left(\frac{di}{dt}\right)_{\text{dr}} = \frac{\mathcal{K}\rho_g \mathcal{R}^{5/2} \sqrt{1-e^2} \cos(f+\omega)}{a n R \rho (1+e \cos f)} \times \left\{ v_{gz} \cos i - v_{gy} \sin i \cos \Omega + v_{gx} \sin i \sin \Omega \right\}, \quad (82)$$

$$\left(\frac{d\Omega}{dt}\right)_{\text{dr}} = \frac{\mathcal{K}\rho_g \mathcal{R}^{5/2} \sqrt{1-e^2} \sin(f+\omega)}{a n R \rho (1+e \cos f)} \times \left\{ v_{gz} \cot i - v_{gy} \cos \Omega + v_{gx} \sin \Omega \right\}, \quad (83)$$

$$\left(\frac{d\omega}{dt}\right)_{\text{dr}} = \frac{\mathcal{K}\rho_g \mathcal{R}^{5/2}}{2naR\rho e \sqrt{1-e^2} (1+e \cos f)} \times \left\{ -a n \sqrt{1-e^2} (C_2 C_7 - C_1 C_9) - (1-e^2) \right. \\ \left[v_{gz} (C_9 \sin i + 2e \cos i \cot i \sin(f+\omega)) \right. \\ \left. - v_{gy} [-\cos i \cos \Omega (C_9 - 2e \sin(f+\omega)) - C_7 \sin \Omega] \right. \\ \left. \left. + v_{gx} [-\cos i \sin \Omega (C_9 - 2e \sin(f+\omega)) + C_7 \cos \Omega] \right] \right\}. \quad (84)$$

4.2.6 Averaged equations

The unaveraged equations demonstrated exactly how the osculating orbital elements change at a given point in time, and most practically, along a single orbit. Averaging over these equations would require additional assumptions, which we do not make here. One can, for example, assume a spherically symmetric wind (as in equation 54) and then some particular analytical prescription for stellar mass loss to treat the variation of \vec{v}_g . However, even with those assumptions, performing averaging over variables such as \mathcal{R} (applicable in the Stokes regime, with $Re > 1$) becomes computationally prohibitive.

4.3 Radiation equations

The equations of motion due to radiative effects (from equation 29) are too complex to be reasonably expressed in osculating orbital elements due to the Yarkovsky contribution. Because the diurnal Yarkovsky acceleration contains an explicit dependence on s , one must also treat the evolution of the target's spin. We can do so through equation (3) only if we assume a slow rate of change. Further, because the seasonal Yarkovsky contribution is an explicit function of the specific angular momentum through equations (14), (17), (18) and (20), the final result is unmanageable even if the diurnal contribution is neglected.

Nevertheless, our perturbation method is sufficient for the purposes of this paper, as we aim to place bounds on the motion and not model any particular system. Consequently, when deriving the perturbation equations below, we assume that the matrix elements of \mathbb{Q} are independent of position and velocity.

4.3.1 Auxiliary expressions

Even with this assumption, the final resulting equations are long. However, we have discovered that they can be expressed compactly by using a smart choice of auxiliary variables. First we define two additional C variables that represent commonly occurring quantities in the equations of motion of our problem.

$$\begin{aligned} C_{10} &\equiv -3e \sin \omega - 2 \sin(f + \omega) + e \sin(2f + \omega), \\ C_{11} &\equiv -3e \cos \omega - 2 \cos(f + \omega) + e \cos(2f + \omega). \end{aligned} \quad (85)$$

Also, we found that one quantity which appears in all of the terms that are proportional to $1/c$ is

$$\begin{aligned} \vec{D}_c &\equiv -C_3 \begin{pmatrix} Q_{11} \\ Q_{21} \\ Q_{31} \end{pmatrix} + C_4 \begin{pmatrix} Q_{12} \\ Q_{22} \\ Q_{32} \end{pmatrix} \\ &+ \sin i \sin(f + \omega) \begin{pmatrix} Q_{13} \\ Q_{23} \\ Q_{33} \end{pmatrix}. \end{aligned} \quad (86)$$

A quantity appearing in all the terms that are proportional to $1/c^2$ is

$$\begin{aligned} \vec{D}_{c^2} &\equiv -(C_{10} \cos \Omega + C_{11} \cos i \sin \Omega) \begin{pmatrix} Q_{11} \\ Q_{21} \\ Q_{31} \end{pmatrix} \\ &- (C_{10} \sin \Omega - C_{11} \cos i \cos \Omega) \begin{pmatrix} Q_{12} \\ Q_{22} \\ Q_{32} \end{pmatrix} \\ &+ C_{11} \sin i \begin{pmatrix} Q_{13} \\ Q_{23} \\ Q_{33} \end{pmatrix} \end{aligned} \quad (87)$$

Terms specific to the orbital element expressions are

$$\vec{D}_a \equiv \begin{pmatrix} -C_2 \cos \Omega - C_1 \sin \Omega \cos i \\ -C_2 \sin \Omega + C_1 \cos \Omega \cos i \\ C_1 \sin i \end{pmatrix}, \quad (88)$$

$$\vec{D}_e \equiv \begin{pmatrix} -C_5 \cos \Omega - C_6 \sin \Omega \cos i \\ -C_5 \sin \Omega + C_6 \cos \Omega \cos i \\ C_6 \sin i \end{pmatrix}, \quad (89)$$

$$\vec{D}_\Omega \equiv \begin{pmatrix} \sin \Omega \\ -\cos \Omega \\ \cot i \end{pmatrix}, \quad (90)$$

$$\vec{D}_i = \sin i \vec{D}_\Omega, \quad (91)$$

$$\vec{D}_\omega \equiv \begin{pmatrix} -C_7 \cos \Omega + C_8 \sin \Omega \cos i \\ -C_7 \sin \Omega - C_8 \cos \Omega \cos i \\ -C_9 \csc i + C_8 \cos i \cot i \end{pmatrix}. \quad (92)$$

4.3.2 Unaveraged equations

Equipped with the above auxiliary variables, the complete final equations of motion entirely in orbital elements are

$$\left(\frac{da}{dt} \right)_{\text{ra}} = \left(\frac{1}{c} \right) \frac{AL(1+e \cos f)^2}{2\pi m n a^2 (1-e^2)^{5/2}} (\vec{D}_c \cdot \vec{D}_a)$$

$$+ \left(\frac{1}{c^2} \right) \frac{AL(1+e \cos f)^2}{4\pi m a (1-e^2)^3} (\vec{D}_{c^2} \cdot \vec{D}_a), \quad (93)$$

$$\begin{aligned} \left(\frac{de}{dt} \right)_{\text{ra}} &= \left(\frac{1}{c} \right) \frac{AL(1+e \cos f)}{8\pi m n a^3 (1-e^2)^{3/2}} (\vec{D}_c \cdot \vec{D}_e) \\ &+ \left(\frac{1}{c^2} \right) \frac{AL(1+e \cos f)}{16\pi m a^2 (1-e^2)^2} (\vec{D}_{c^2} \cdot \vec{D}_e), \end{aligned} \quad (94)$$

$$\begin{aligned} \left(\frac{di}{dt} \right)_{\text{ra}} &= \left(\frac{1}{c} \right) \frac{AL(1+e \cos f) \cos(f + \omega)}{4\pi m n a^3 (1-e^2)^{3/2}} (\vec{D}_c \cdot \vec{D}_i) \\ &+ \left(\frac{1}{c^2} \right) \frac{AL(1+e \cos f) \cos(f + \omega)}{8\pi m a^2 (1-e^2)^2} (\vec{D}_{c^2} \cdot \vec{D}_i), \end{aligned} \quad (95)$$

$$\begin{aligned} \left(\frac{d\Omega}{dt} \right)_{\text{ra}} &= \left(\frac{1}{c} \right) \frac{AL(1+e \cos f) \sin(f + \omega)}{4\pi m n a^3 (1-e^2)^{3/2}} (\vec{D}_c \cdot \vec{D}_\Omega) \\ &+ \left(\frac{1}{c^2} \right) \frac{AL(1+e \cos f) \sin(f + \omega)}{8\pi m a^2 (1-e^2)^2} (\vec{D}_{c^2} \cdot \vec{D}_\Omega), \end{aligned} \quad (96)$$

$$\begin{aligned} \left(\frac{d\omega}{dt} \right)_{\text{ra}} &= \left(\frac{1}{c} \right) \frac{AL(1+e \cos f)}{8\pi m n a^3 e (1-e^2)^{3/2}} (\vec{D}_c \cdot \vec{D}_\omega) \\ &+ \left(\frac{1}{c^2} \right) \frac{AL(1+e \cos f)}{16\pi m a^2 e (1-e^2)^2} (\vec{D}_{c^2} \cdot \vec{D}_\omega). \end{aligned} \quad (97)$$

Equations (93)-(97) are convenient because all of the \vec{D} auxiliary variables, which are on the order of unity, are isolated. They also show that the amplitudes of the orbital element rates of changes are independent of i , and Ω . Further, for many purposes, the $1/c^2$ term may be neglected.

4.3.3 Unaveraged equations with no Yarkovsky

When the Yarkovsky effect is “off”, which typically occurs for targets with diameters less than 1 cm-1 m, a significant simplification occurs. Now, \mathbb{Q} is a diagonal matrix, and we can convert that into a scalar. Consequently, equation (29) becomes

$$\left(\frac{d\vec{v}}{dt} \right)_{\text{ra}} \Big|_{\mathbb{Y}=0} = \frac{AL(Q_{\text{abs}} + Q_{\text{ref}})}{4\pi m c r^2} \vec{L}. \quad (98)$$

Subsequently, the equations of motion simplify to the following relations

$$\begin{aligned} \left(\frac{da}{dt} \right)_{\text{ra}} \Big|_{\mathbb{Y}=0} &= \frac{AL(Q_{\text{abs}} + Q_{\text{ref}})(1+e \cos f)^2}{2\pi m (1-e^2)^3} \\ &\times \left[\frac{e\sqrt{1-e^2} \sin f}{n a^2} \left(\frac{1}{c} \right) \right. \\ &\left. + \frac{-2-3e^2-4e \cos f + e^2 \cos(2f)}{2a} \left(\frac{1}{c^2} \right) \right], \end{aligned} \quad (99)$$

$$\left(\frac{de}{dt} \right)_{\text{ra}} \Big|_{\mathbb{Y}=0} = \frac{AL(Q_{\text{abs}} + Q_{\text{ref}})(1+e \cos f)^2}{4\pi m (1-e^2)^{3/2}}$$

$$\times \left[\frac{\sin f}{na^3} \left(\frac{1}{c} \right) + \frac{-4 \cos f + e (\cos(2f) - 5)}{2a^2 \sqrt{1-e^2}} \left(\frac{1}{c^2} \right) \right], \quad (100)$$

$$\left(\frac{di}{dt} \right)_{\text{ra}} \Big|_{\mathbb{Y}=0} = \left(\frac{d\Omega}{dt} \right)_{\text{ra}} \Big|_{\mathbb{Y}=0} = 0, \quad (101)$$

$$\left(\frac{d\omega}{dt} \right)_{\text{ra}} \Big|_{\mathbb{Y}=0} = \left(\frac{d\varpi}{dt} \right)_{\text{ra}} \Big|_{\mathbb{Y}=0} = -\frac{AL(Q_{\text{abs}} + Q_{\text{ref}})(1 + e \cos f)^2}{4\pi m e (1 - e^2)^{3/2}} \times \left[\frac{\cos f}{na^3} \left(\frac{1}{c} \right) + \frac{\sin f (2 - e \cos f)}{a^2 \sqrt{1 - e^2}} \left(\frac{1}{c^2} \right) \right]. \quad (102)$$

For pebbles which are subject to intense radiation, equations (98)-(102) describe their evolution due to this perturbation exactly. For asteroids, however, equations (93)-(97) should be used instead. For particular models which require a detailed analysis of the perturbation at the pericentre or the stationary points of the motion along an orbit, equations (98)-(102) are compact enough to allow for an analysis similar to the one by Veras (2014b).

4.3.4 Averaged equations

Now we return to the general equations in (93)-(97) and average over them. Integrating these equations yields long expressions. We write out these expressions in the appendix (with the $1/c$ term only) because they can be cast in a revealing form.

Just by inspection of equations (A2)-(A6), one can see that when the Yarkovsky effect does not operate (e.g. and the off-diagonal terms of \mathbb{Q} become zero) all of the $(1/c)$ are zeroed out. Therefore, radiative treatments which do not include the Yarkovsky effect are potentially missing an important perturbation in the system!

Now we quantify this statement. Because the matrices in Appendix A are all of order unity, we can write

$$\left\langle \left(\frac{da}{dt} \right)_{\text{ra}} \right\rangle = \mathcal{O} \left(\frac{1}{c} \frac{AL}{4\pi m n a^2} \right), \quad (103)$$

$$\left\langle \left(\frac{de}{dt} \right)_{\text{ra}} \right\rangle = \mathcal{O} \left(\frac{1}{c} \frac{AL}{8\pi m n a^3} \right), \quad (104)$$

$$\left\langle \left(\frac{di}{dt} \right)_{\text{ra}} \right\rangle = \mathcal{O} \left(\frac{1}{c} \frac{AL}{8\pi m n a^3} \right), \quad (105)$$

$$\left\langle \left(\frac{d\Omega}{dt} \right)_{\text{ra}} \right\rangle = \mathcal{O} \left(\frac{1}{c} \frac{AL}{8\pi m n a^3} \right), \quad (106)$$

$$\left\langle \left(\frac{d\omega}{dt} \right)_{\text{ra}} \right\rangle = \mathcal{O} \left(\frac{1}{c} \frac{AL}{32\pi m n a^3} \right). \quad (107)$$

Isolating the rate of change of eccentricity with time yields

$$\mathcal{O} \left(\frac{1}{c} \frac{AL}{8\pi m n a^3} \right) \sim \frac{0.08}{\text{Myr}} \left(\frac{M_\star}{1M_\odot} \right)^{-1/2} \left(\frac{\rho}{2 \text{ g/cm}^3} \right)^{-1} \times \left(\frac{R}{1 \text{ km}} \right)^{-1} \left(\frac{a}{5 \text{ au}} \right)^{-3/2} \left(\frac{L}{10^3 L_\odot} \right). \quad (108)$$

In other words, the Yarkovsky effect alone can fling an initially near-circular asteroid out of the system after about 10 Myr! This case however assumes that changes in the asteroid's rotation state from YORP and close encounters with the star are neglected. For highly eccentric orbits, both effects are likely to cause a substantial change in the spin state of the body, which – in turn – could eventually eliminate the Yarkovsky effect. Also, the interplay between the asteroid's rotation and the stellar wind should be investigated.

In order to compare to the non-Yarkovsky term (which includes Poynting-Robertson drag and “radiation pressure”), note the following standard result (also seen in equation 112) but applied to GB stars

$$\mathcal{O} \left(\frac{1}{c^2} \frac{5AL}{8\pi m a^2} \right) \sim \frac{1.8 \times 10^{-5}}{\text{Myr}} \left(\frac{\rho}{2 \text{ g/cm}^3} \right)^{-1} \times \left(\frac{R}{1 \text{ km}} \right)^{-1} \left(\frac{a}{5 \text{ au}} \right)^{-2} \left(\frac{L}{10^3 L_\odot} \right), \quad (109)$$

which is over three orders of magnitude less powerful.

Although the evolution due to time-dependent radiation is more complex than equations (108)-(109) suggest (see Appendix A), the sheer magnitude of equation (108) reveals something fundamental about the physics in these systems. Possibilities include (1) that asteroids in fact escape GB systems en masse, with or without the help of mass loss, depending on the stellar wind evolution, (2) asteroids survive but are widely dispersed in eccentricity and inclination, (3) the temporal variations in the individual elements of \mathbb{Q} cancel out secular changes in the orbits, and (4) the value of k is typically exceptionally low and/or the value of Q_{ref} is within a tiny fraction of unity so that Yarkovsky is quashed. This degeneracy in interpretation cannot be broken without adopting a detailed internal model of the target and in particular how its incoming radiation is redistributed and how its spin axis changes with time. Such a model is well beyond the scope of this paper.

Further, and unhelpfully, we can pose arguments against all four possibilities. Possibility (1) is unlikely because, as described in Section 1, asteroids represent the most likely candidate for the WD pollution that is currently observed. Possibility (2) might be prevented from occurring due to collisions with planets⁷, other asteroids or smaller bodies, depending on the architecture of the exosystem in question. For possibility (3), the equations in Appendix A demonstrate that even if the off-diagonal nonzero elements of \mathbb{Q} cancel one another, other combinations of elements will not cancel. Although the equations were derived assuming position and velocity-independent values of \mathbb{Q} , the current equations represent an accurate evolutionary picture at system snapshots when the seasonal component is neglected. Finally, the extreme values of k and Q_{ref} that are required for possibility (4) do not conform to what we observe in the Solar system.

We can place these results in the context of the asteroids observed in the Solar System. These asteroids, exposed to the relatively weak MS luminosity of a $1M_\odot$ star, can experience a significant drift in eccentricity (~ 0.1) over 1 Gyr (e.g. Figs. 7-8

⁷ Alternatively, distant planet-asteroid interactions due to post-MS planet-planet scattering could repress or excite both eccentricity and inclination (Veras & Armitage 2005, 2006; Raymond et al. 2010; Matsumura et al. 2013).

of Vokrouhlický et al. 2006). Because these Eros family asteroids are located at $a \approx 3$ au and with $R > 3.5$ km, this comparison yields good agreement with equation (108). Note that the semi-major axis drift in these asteroids over this time period is just 0.1 au. By estimating the semimajor axis drift from equation (103), we obtain

$$\mathcal{O}\left(\frac{1}{c} \frac{AL}{4\pi mna^2}\right) \sim \frac{0.81 \text{ au}}{\text{Myr}} \left(\frac{M_\star}{1M_\odot}\right)^{-1/2} \left(\frac{\rho}{2 \text{ g/cm}^3}\right)^{-1} \times \left(\frac{R}{1 \text{ km}}\right)^{-1} \left(\frac{a}{5 \text{ au}}\right)^{-1/2} \left(\frac{L}{10^3 L_\odot}\right). \quad (110)$$

For a Solar-type star ($L = L_\odot$), this level of drift is within the same order of magnitude as the maximum that is observed and predicted in the Solar system (e.g. Farinella et al. 1998; Bottke et al. 2006; Vokrouhlický et al. 2006).

4.3.5 Averaged equations with no Yarkovsky

Recall that when Yarkovsky is not active, we are still left with (much smaller) radiative perturbations from Poynting-Robertson drag and radiation pressure. We compute exactly these less-powerful ($1/c^2$) terms to be

$$\left\langle \left(\frac{da}{dt} \right)_{\text{ra}} \right|_{\mathbb{Y}=0} = - \left(\frac{1}{c^2} \right) \frac{AL(Q_{\text{abs}} + Q_{\text{ref}})(2 + 3e^2)}{4\pi ma(1 - e^2)^{3/2}}, \quad (111)$$

$$\left\langle \left(\frac{de}{dt} \right)_{\text{ra}} \right|_{\mathbb{Y}=0} = - \left(\frac{1}{c^2} \right) \frac{5AL(Q_{\text{abs}} + Q_{\text{ref}})e}{8\pi ma^2\sqrt{1 - e^2}}, \quad (112)$$

$$\left\langle \left(\frac{di}{dt} \right)_{\text{ra}} \right|_{\mathbb{Y}=0} = \left\langle \left(\frac{d\Omega}{dt} \right)_{\text{ra}} \right|_{\mathbb{Y}=0} = 0, \quad (113)$$

$$\left\langle \left(\frac{d\omega}{dt} \right)_{\text{ra}} \right|_{\mathbb{Y}=0} = \left\langle \left(\frac{d\varpi}{dt} \right)_{\text{ra}} \right|_{\mathbb{Y}=0} = 0. \quad (114)$$

Equations (111)-(112), with a coefficient of $1/c^2$, reproduce now-standard results from Wyatt & Whipple (1950). Their relative importance is showcased by comparing them to equations (A2)-(A6), which instead harbour terms with a coefficient of $1/c$. Consequently, the Yarkovsky effect *when active, dominates the target's secular evolution over other radiative effects*. Yarkovsky causes changes that are absent from immediately reflected radiation. Equations (113)-(114) are also important because they reveal that when Yarkovsky turns on, a target will drift out of the orbital plane that it previously occupied.

5 SUMMARY

Post-main-sequence stellar radiation and winds play a decisive role in determining the final orbital states of asteroids, pebbles and smaller particles. *Any bodies smaller than about 1000 km will be significantly affected by forces other than gravity during GB evolution.* This paper has quantified this main conclusion through two avenues: a rough comparison of the instantaneous accelerations caused by mass loss, wind drag and radiation (Section 3) and a precise detailing of the orbital element equations

of motions for these forces both during a single orbit and over secular timescales (Section 4 + Appendix).

Several ancillary results are widely applicable to planetary systems at all stages of evolution, including pre-MS and beginning MS stages. We summarize these results as (1) a self-consistent framework to treat Poynting-Robertson drag, radiation pressure and the Yarkovsky effect (equation 29), (2) an orbital element characterization of the Reynolds number for stellar winds (equations 39, 49-53), (3) the complete set of orbital element evolution equations for a particle dragged by gas in the Epstein and Stokes regimes (equations 70-84), (4) the complete unaveraged set of equations due to radiative perturbations assuming position and velocity-independent diurnal and seasonal Yarkovsky components (equations 93-97), and (5) the leading order of the averaged set of these equations (A2-A6) when the seasonal Yarkovsky component is negligible. This last set, along with equations (108)-(109), demonstrate the potential for the Yarkovsky effect alone to dominate the eccentricity and inclination evolution of bodies larger than 1-10 m.

Detailed models of the time-varying stellar wind and the physical properties of an orbiting body are required to determine its ultimate fate. Here, we have provided a set of machinery in which such models may be incorporated.

ACKNOWLEDGMENTS

We thank the referee for a thorough, probing report that has improved the manuscript. We also thank Holly Capelo, Alan W. Harris and Anders Johansen for useful discussions. BTG and DV benefited by support by the European Union through ERC grant number 320964. SE would like to acknowledge the support of the NEOSShield project funded by the European Union Seventh Framework Program (FP7/2007-2013) under grant agreement no. 282703 (NEOSShield) as well as Paris Observatory's ESTERS (Environnement Spatial de la Terre : Recherche & Surveillance) travel grants.

APPENDIX A: EXPLICIT EXPRESSIONS FOR AVERAGED YARKOVSKY EQUATIONS

Here we write out the expressions from equations (103)-(107), and do so in a form which elucidates how the leading order term ($1/c$) vanishes when the Yarkovsky effect is turned off. We remind the reader that an implicit assumption in these equations is that the components of \mathbb{Q} are independent of \vec{r} and \vec{v} .

When the Yarkovsky effect plays no role in the motion, then all of the off-diagonal terms of \mathbb{Q} vanish, such that $\mathbb{Q}_{12} = \mathbb{Q}_{21} = \mathbb{Q}_{13} = \mathbb{Q}_{31} = \mathbb{Q}_{23} = \mathbb{Q}_{32} = 0$. Further, the diagonal terms become equal, so that $\mathbb{Q}_{11} = \mathbb{Q}_{22} = \mathbb{Q}_{33}$. Also, in the subsequent expressions, we compress commonly-occurring eccentricity-based quantities as

$$\kappa \equiv -2 + e^2 + 2\sqrt{1 - e^2}. \quad (\text{A1})$$

The final expressions are

$$\left\langle \left(\frac{da}{dt} \right)_{\text{ra}} \right\rangle = \left(\frac{1}{c} \right) \frac{AL}{4\pi mna^2(1 - e^2)} \begin{pmatrix} \mathbb{Q}_{21} - \mathbb{Q}_{12} \\ \mathbb{Q}_{32} - \mathbb{Q}_{23} \\ \mathbb{Q}_{31} - \mathbb{Q}_{13} \end{pmatrix} \cdot \begin{pmatrix} \cos i \\ \sin i \sin \Omega \\ \sin i \cos \Omega \end{pmatrix} + \mathcal{O} \left(\frac{1}{c^2} \frac{AL}{ma} \right), \quad (\text{A2})$$

$$\begin{aligned} \left\langle \left(\frac{de}{dt} \right)_{\text{ra}} \right\rangle &= \left(\frac{1}{c} \right) \frac{AL(1 - \sqrt{1 - e^2})}{8\pi mna^3 e} \begin{pmatrix} \mathbb{Q}_{21} - \mathbb{Q}_{12} \\ \mathbb{Q}_{32} - \mathbb{Q}_{23} \\ \mathbb{Q}_{31} - \mathbb{Q}_{13} \end{pmatrix} \cdot \begin{pmatrix} \cos i \\ \sin i \sin \Omega \\ \sin i \cos \Omega \end{pmatrix} \\ &+ \left(\frac{1}{c} \right) \frac{AL\sqrt{1 - e^2}\kappa}{8\pi mna^3 e^3} \begin{pmatrix} \mathbb{Q}_{12} + \mathbb{Q}_{21} \\ \mathbb{Q}_{23} + \mathbb{Q}_{32} \\ \mathbb{Q}_{13} + \mathbb{Q}_{31} \\ \mathbb{Q}_{22} - \mathbb{Q}_{11} \\ \mathbb{Q}_{11} + \mathbb{Q}_{22} - 2\mathbb{Q}_{33} \end{pmatrix} \cdot \begin{pmatrix} \cos i \cos 2\omega \cos 2\Omega - (1 + \cos^2 i) \cos \Omega \sin 2\omega \sin \Omega \\ \sin i [\cos i \cos \Omega \sin 2\omega + \cos 2\omega \sin \Omega] \\ \sin i [-\cos i \sin \Omega \sin 2\omega + \cos 2\omega \cos \Omega] \\ \cos i \cos 2\omega \sin 2\Omega + (1 + \cos^2 i) \cos \Omega \sin 2\omega \sin \Omega \\ -\sin^2 i \sin \omega \cos \omega \end{pmatrix} \\ &+ \mathcal{O} \left(\frac{1}{c^2} \frac{AL}{ma^2} \right), \quad (\text{A3}) \end{aligned}$$

$$\begin{aligned} \left\langle \left(\frac{di}{dt} \right)_{\text{ra}} \right\rangle &= \left(\frac{1}{c} \right) \frac{AL}{8\pi mna^3 e^2 \sqrt{1 - e^2}} \left[\mathbb{Q} \cdot \begin{pmatrix} \sin i \sin \Omega \\ -\sin i \cos \Omega \\ \cos i \end{pmatrix} \right] \cdot \begin{pmatrix} e^2 \cos \Omega + \kappa (\cos i \sin 2\omega \sin \Omega - \cos 2\omega \cos \Omega) \\ e^2 \sin \Omega - \kappa (\cos i \sin 2\omega \cos \Omega + \cos 2\omega \sin \Omega) \\ -\kappa \sin 2\omega \sin i \end{pmatrix} \\ &+ \mathcal{O} \left(\frac{1}{c^2} \frac{AL}{ma^2} \right), \quad (\text{A4}) \end{aligned}$$

$$\begin{aligned} \left\langle \left(\frac{d\Omega}{dt} \right)_{\text{ra}} \right\rangle &= \left(\frac{1}{c} \right) \frac{AL}{8\pi mna^3 e^2 \sqrt{1 - e^2}} \left[\mathbb{Q} \cdot \begin{pmatrix} \sin \Omega \\ -\cos \Omega \\ \cot i \end{pmatrix} \right] \cdot \begin{pmatrix} -e^2 \cos i \sin \Omega - \kappa (\cos i \cos 2\omega \sin \Omega + \sin 2\omega \cos \Omega) \\ e^2 \cos i \cos \Omega + \kappa (\cos i \cos 2\omega \cos \Omega - \sin 2\omega \sin \Omega) \\ e^2 \sin i + \kappa \cos 2\omega \sin i \end{pmatrix} \\ &+ \mathcal{O} \left(\frac{1}{c^2} \frac{AL}{ma^2} \right), \quad (\text{A5}) \end{aligned}$$

$$\left\langle \left(\frac{d\omega}{dt} \right)_{\text{ra}} \right\rangle = \left(\frac{1}{c} \right) \frac{AL}{32\pi mna^3 e^4 \sqrt{1 - e^2}} \cdot \begin{pmatrix} \mathbb{Q}_{12} - \mathbb{Q}_{21} \\ \mathbb{Q}_{23} - \mathbb{Q}_{32} \\ \mathbb{Q}_{13} - \mathbb{Q}_{31} \\ \mathbb{Q}_{12} + \mathbb{Q}_{21} \\ \mathbb{Q}_{23} + \mathbb{Q}_{32} \\ \mathbb{Q}_{13} + \mathbb{Q}_{31} \\ \mathbb{Q}_{11} + \mathbb{Q}_{22} \\ \mathbb{Q}_{11} - \mathbb{Q}_{22} \\ \mathbb{Q}_{11} + \mathbb{Q}_{22} - 2\mathbb{Q}_{33} \end{pmatrix} \cdot \begin{pmatrix} \Upsilon_1 \\ \Upsilon_2 \\ \Upsilon_3 \\ \Upsilon_4 \\ \Upsilon_5 \\ \Upsilon_6 \\ \Upsilon_7 \\ \Upsilon_8 \\ \Upsilon_9 \end{pmatrix} + \mathcal{O} \left(\frac{1}{c^2} \frac{AL}{ma^2} \right) \quad (\text{A6})$$

where the auxiliary Υ variables are long explicit functions of (e, i, Ω, ω) . We do not write out these functions here but are happy to provide them to interested readers.

REFERENCES

- Aannestad, P. A., Kenyon, S. J., Hammond, G. L., & Sion, E. M. 1993, *AJ*, 105, 1033
- Adachi, I., Hayashi, C., & Nakazawa, K. 1976, *Progress of Theoretical Physics*, 56, 1756
- Adamów, M., Niedzielski, A., Villaver, E., Nowak, G., & Wolszczan, A. 2012, *ApJL*, 754, LL15
- Adamów, M., Niedzielski, A., Villaver, E., Wolszczan, A., & Nowak, G. 2014, *A&A*, 569, AA55
- Barstow, M. A., Barstow, J. K., Casewell, S. L., Holberg, J. B., & Hubeny, I. 2014, *MNRAS*, 440, 1607
- Bear, E., & Soker, N. 2013, *New Astronomy*, 19, 56
- Beaugé, C., Leiva, A. M., Haghighipour, N., & Otto, J. C. 2010, *MNRAS*, 408, 503
- Becklin, E. E., Farihi, J., Jura, M., et al. 2005, *ApJL*, 632, L119
- Bergfors, C., Farihi, J., Dufour, P., & Rocchetto, M. 2014, *MNRAS*, 444, 2147
- Bladh, S., Höfner, S. 2012, *A&A*, 546, AA76
- Bonsor, A., & Wyatt, M. 2010, *MNRAS*, 409, 1631
- Bonsor, A., Mustill, A. J., & Wyatt, M. C. 2011, *MNRAS*, 414, 930
- Bonsor, A., Kennedy, G. M., Crepp, J. R., et al. 2013, *MNRAS*, 431, 3025
- Bonsor, A., Kennedy, G. M., Wyatt, M. C., Johnson, J. A., & Sibthorpe, B. 2014, *MNRAS*, 437, 3288
- Bottke, W. F., Jr., Vokrouhlický, D., Rubincam, D. P., & Nesvorný, D. 2006, *Annual Review of Earth and Planetary Sciences*, 34, 157
- Bottke, W. F., Vokrouhlický, D., Walsh, K. J., et al. 2015, *Icarus*, 247, 191
- Brinkworth, C. S., Gänsicke, B. T., Marsh, T. R., Hoard, D. W., & Tappert, C. 2009, *ApJ*, 696, 1402
- Brinkworth, C. S., Gänsicke, B. T., Girven, J. M., et al. 2012, *ApJ*, 750, 86
- Brož, M. 2006, Ph.D. Thesis
- Burns, J. A., Lamy, P. L., & Soter, S. 1979, *Icarus*, 40, 1
- Burns, J. A., Lamy, P. L., & Soter, S. 2014, *Icarus*, 232, 263
- Ciceri, S., Lillo-Box, J., Southworth, J., et al. 2015, *A&A*, 573, LL5
- Debes, J. H., Walsh, K. J., & Stark, C. 2012, *ApJ*, 747, 148
- Deprit, A. 1983, *Celestial Mechanics*, 31, 1
- Dong, R., Wang, Y., Lin, D. N. C., & Liu, X.-W. 2010, *ApJ*, 715, 1036
- Dufour, P., Kilic, M., Fontaine, G., et al. 2012, *ApJ*, 749, 6
- Efroimsky, M. 2005, *Annals of the New York Academy of Sciences*, 1065, 346
- Farihi, J., Jura, M., & Zuckerman, B. 2009, *ApJ*, 694, 805
- Farihi, J., Barstow, M. A., Redfield, S., Dufour, P., & Hambly, N. C. 2010, *MNRAS*, 404, 2123
- Farihi, J., Gänsicke, B. T., Steele, P. R., et al. 2012, *MNRAS*, 421, 1635
- Farihi, J., Gänsicke, B. T., & Koester, D. 2013, *Science*, 342, 218
- Farinella, P., Vokrouhlický, D., & Hartmann, W. K. 1998, *Icarus*, 132, 378
- Frewen, S. F. N., & Hansen, B. M. S. 2014, *MNRAS*, 439, 2442
- Friedrich, S., Jordan, S., & Koester, D. 2004, *A&A*, 424, 665
- Gänsicke, B. T., Marsh, T. R., Southworth, J., & Rebassa-Mansergas, A. 2006, *Science*, 314, 1908
- Gänsicke, B. T., Marsh, T. R., & Southworth, J. 2007, *MNRAS*, 380, L35
- Gänsicke, B. T., Koester, D., Marsh, T. R., Rebassa-Mansergas, A., & Southworth, J. 2008, *MNRAS*, 391, L103
- Gänsicke, B. T. 2011, *American Institute of Physics Conference Series*, 1331, 211
- Gänsicke, B. T., Koester, D., Farihi, J., et al. 2012, *MNRAS*, 424, 333
- Garaud, P., Barrière-Fouchet, L., & Lin, D. N. C. 2004, *ApJ*, 603, 292
- Gibbons, P. G., Rice, W. K. M., & Mamatsashvili, G. R. 2012, *MNRAS*, 426, 1444
- Graham, J. R., Matthews, K., Neugebauer, G., & Soifer, B. T. 1990, *ApJ*, 357, 216
- Gurfil, P. 2007, *Acta Astronautica*, 60, 61
- Hadjidemetriou, J. D. 1963, *Icarus*, 2, 440
- Harris, A. W. 1994, *Icarus*, 107, 209
- Hamilton, D. P. 1993, *Icarus*, 101, 244
- Howe, A. R., & Rafikov, R. R. 2014, *ApJ*, 781, 52
- Hurley, J. R., Pols, O. R., & Tout, C. A. 2000, *MNRAS*, 315, 543
- Iwasaki, K., Emori, H., Nakazawa, K., & Tanaka, H. 2002, *PASJ*, 54, 471
- Jacobson, S. A., Marzari, F., Rossi, A., Scheeres, D. J., & Davis, D. R. 2014, *MNRAS*, 439, L95
- Jura, M. 2003, *ApJL*, 584, L91
- Jura, M. 2006, *ApJ*, 653, 613
- Jura, M., & Xu, S. 2010, *AJ*, 140, 1129
- Jura, M., & Xu, S. 2012, *AJ*, 143, 6
- Kilic, M., von Hippel, T., Leggett, S. K., & Winget, D. E. 2005, *ApJL*, 632, L115
- Kilic, M., & Redfield, S. 2007, *ApJ*, 660, 641
- Klačka, J., Petržala, J., Pástor, P., & Kómar, L. 2014, *Icarus*, 232, 249
- Koester, D., Gänsicke, B. T., & Farihi, J. 2014, *A&A*, 566, A34
- Kryszczyńska, A. 2013, *A&A*, 551, AA102
- Lillo-Box, J., Barrado, D., Henning, T., et al. 2014, *A&A*, 568, LL1
- Lorén-Aguilar, P., & Bate, M. R. 2014, *MNRAS*, 443, 927
- Lowry, S. C., Weissman, P. R., Duddy, S. R., et al. 2014, *A&A*, 562, AA48
- Lupishko, D., & Tielieusova, I. 2014, *Meteoritics and Planetary Science*, 49, 80
- Manser, C. et al. 2015, In Preparation
- Matsumura, S., Ida, S., & Nagasawa, M. 2013, *ApJ*, 767, 129
- Melis, C., Jura, M., Albert, L., Klein, B., & Zuckerman, B. 2010, *ApJ*, 722, 1078
- Melis, C., Dufour, P., Farihi, J., et al. 2012, *ApJL*, 751, L4
- Mignard, F. 1984, *IAU Colloq. 75: Planetary Rings*, 333
- Murray, C. D., & Dermott, S. F. 1999, *Solar system dynamics*
- Mustill, A. J., Marshall, J. P., Villaver, E., et al. 2013, *MNRAS*, 436, 2515
- Mustill, A. J., Veras, D., & Villaver, E. 2014, *MNRAS*, 437, 1404
- Niedzielski, A., Villaver, E., Wolszczan, A., et al. 2015, *A&A*, 573, AA36
- Nowak, G., Niedzielski, A., Wolszczan, A., Adamów, M., & Maciejewski, G. 2013, *ApJ*, 770, 53
- O’Keefe, J. A., *Tektites and Their Origin*, Elsevier Sci., New York, 1976.

- Omarov, T. B. 1962, *Izv. Astrofiz. Inst. Acad. Nauk. KazSSR*, 14, 66
- Öpik, E. J. 1951, *Proc. Roy. Irish Acad.* 54, 165
- Ortiz, M., Gandolfi, D., Reffert, S., et al. 2015, *A&A*, 573, LL6
- Owocicki, S. 2004, *EAS Publications Series*, 13, 163
- Owocicki, S. 2013, *Planets, Stars and Stellar Systems. Volume 4: Stellar Structure and Evolution*, 735
- Owocicki, S. 2014, arXiv:1409.2084
- Paddack, S. J. 1969, *JGR*, 74, 4379
- Pástor, P. 2014, *Celestial Mechanics and Dynamical Astronomy*, 120, 77
- Peterson, C. 1976, *Icarus*, 29, 91
- Polishook, D. 2014, *Icarus*, 241, 79
- Porter, S., & Grundy, W. 2014, arXiv:1403.4873, In Press, *Icarus*
- Poynting, J. H. 1904, *Royal Society of London Philosophical Transactions Series A*, 202, 525
- Raddi, R., Gänsicke, B. T., Koester, D., Farihi, J., Hermes, J.J., Scaringi, S., Breedt, E., Girven, J. 2015, *MNRAS In Press*, arXiv: 1503.07864
- Rafikov, R. R. 2011a, *MNRAS*, 416, L55
- Rafikov, R. R. 2011b, *ApJL*, 732, L3
- Rafikov, R. R., & Garmilla, J. A. 2012, *ApJ*, 760, 123
- Radzievskii, V. V. 1954, *Dokl. Akad Nauk SSSR*, 97, 49
- Raymond, S. N., Armitage, P. J., & Gorelick, N. 2010, *ApJ*, 711, 772
- Reach, W. T., Kuchner, M. J., von Hippel, T., et al. 2005, *ApJL*, 635, L161
- Robertson, H. P. 1937, *MNRAS*, 97, 423
- Rocchetto, M., Farihi, J., Gänsicke, B. T., & Bergfors, C. 2015, *MNRAS*, 449, 574
- Rozitis, B., Duddy, S. R., Green, S. F., & Lowry, S. C. 2013, *A&A*, 555, AA20
- Sánchez, P., & Scheeres, D. J. 2014, *Meteoritics and Planetary Science*, 49, 788
- Scheeres, D. J. 2007, *Icarus*, 188, 430
- Stone, N., Metzger, B. D., & Loeb, A. 2015, *MNRAS*, 448, 188
- Tadeu dos Santos, M., Correa-Otto, J. A., Michtchenko, T. A., & Ferraz-Mello, S. 2015, *A&A*, 573, AA94
- van de Hulst, H. C. 1981, *New York: Dover*
- Vassiliadis, E., & Wood, P. R. 1993, *ApJ*, 413, 641
- Veras, D., & Armitage, P. J. 2005, *ApJL*, 620, L111
- Veras, D., & Armitage, P. J. 2006, *ApJ*, 645, 1509
- Veras, D., Wyatt, M. C., Mustill, A. J., Bonsor, A., & Eldridge, J. J. 2011, *MNRAS*, 417, 2104
- Veras, D., & Raymond, S. N. 2012, *MNRAS*, 421, L117
- Veras, D., & Tout, C. A. 2012, *MNRAS*, 422, 1648
- Veras, D., & Wyatt, M. C. 2012, *MNRAS*, 421, 2969
- Veras, D., Mustill, A. J., Bonsor, A., & Wyatt, M. C. 2013a, *MNRAS*, 431, 1686
- Veras, D., Hadjidemetriou, J. D., & Tout, C. A. 2013b, *MNRAS*, 435, 2416
- Veras, D., & Evans, N. W. 2013a, *Celestial Mechanics and Dynamical Astronomy*, 115, 123
- Veras, D., & Evans, N. W. 2013b, *MNRAS*, 430, 403
- Veras, D. 2014a, *Celestial Mechanics and Dynamical Astronomy*, 118, 315
- Veras, D. 2014b, *MNRAS*, 442, L71
- Veras, D., Shannon, A., Gänsicke, B. T. 2014a, *MNRAS*, 445, 4175
- Veras, D., Leinhardt, Z. M., Bonsor, A., Gänsicke, B. T. 2014b, *MNRAS*, 445, 2244
- Veras, D., Jacobson, S. A., Gänsicke, B. T. 2014c, *MNRAS*, 445, 2794
- Veras, D., Evans, N. W., Wyatt, M. C., & Tout, C. A. 2014d, *MNRAS*, 437, 1127
- Veras, D., & Gänsicke, B. T. 2015, *MNRAS*, 447, 1049
- Vokrouhlický, D., Brož, M., Morbidelli, A., et al. 2006, *Icarus*, 182, 92
- Voyatzis, G., Hadjidemetriou, J. D., Veras, D., & Varvoglis, H. 2013, *MNRAS*, 430, 3383
- Wang, L., Sato, B., Omiya, M., et al. 2014, arXiv:1409.6081, In Press, *PASJ*
- Wilson, D. J., Gänsicke, B. T., Koester, D., et al. 2014, *MNRAS*, 445, 1878
- Wilson, D. J., Gänsicke, B. T., et al. 2015, Submitted to *MNRAS*
- Wyatt, S. P., & Whipple, F. L. 1950, *ApJ*, 111, 134
- Wyatt, M. C., Farihi, J., Pringle, J. E., & Bonsor, A. 2014, *MNRAS*, 439, 3371
- Xu, S., & Jura, M. 2014, *ApJL*, 792, LL39
- Xu, S., Jura, M., Koester, D., Klein, B., & Zuckerman, B. 2014, *ApJ*, 783, 79
- Yamaguchi, M. S., & Kimura, S. S. 2014, arXiv:1408.4306, In Press *Earth, Planets and Space*
- Zuckerman, B., & Becklin, E. E. 1987, *Nature*, 330, 138
- Zuckerman, B., Koester, D., Reid, I. N., Hünsch, M. 2003, *ApJ*, 596, 477
- Zuckerman, B., Koester, D., Melis, C., Hansen, B. M., & Jura, M. 2007, *ApJ*, 671, 872
- Zuckerman, B., Melis, C., Klein, B., Koester, D., & Jura, M. 2010, *ApJ*, 722, 725